

# UCSF

## UC San Francisco Previously Published Works

### Title

AMPK-mediated potentiation of GABAergic signalling drives hypoglycaemia-provoked spike-wave seizures

### Permalink

<https://escholarship.org/uc/item/78c3t81t>

### Journal

Brain, 145(7)

### ISSN

0006-8950

### Authors

Salvati, Kathryn A  
Ritger, Matthew L  
Davoudian, Pasha A  
[et al.](#)

### Publication Date

2022-07-29

### DOI

10.1093/brain/awac037



### Copyright Information

This work is made available under the terms of a Creative Commons Attribution-NonCommercial License, available at <https://creativecommons.org/licenses/by-nc/4.0/>

Peer reviewed



# AMPK-mediated potentiation of GABAergic signalling drives hypoglycaemia-provoked spike-wave seizures

Kathryn A. Salvati,<sup>1,2</sup> Matthew L. Ritger,<sup>1</sup>  Pasha A. Davoudian,<sup>1,3</sup> Finnegan O'Dell,<sup>1</sup> Daniel R. Wyskiel,<sup>1</sup> George M. P. R. Souza,<sup>1</sup> Adam C. Lu,<sup>1</sup> Edward Perez-Reyes,<sup>1</sup> Joshua C. Drake,<sup>4,5</sup> Zhen Yan<sup>1,5,6,7</sup> and  Mark P. Beenhakker<sup>1</sup>

Metabolism regulates neuronal activity and modulates the occurrence of epileptic seizures. Here, using two rodent models of absence epilepsy, we show that hypoglycaemia increases the occurrence of spike-wave seizures. We then show that selectively disrupting glycolysis in the thalamus, a structure implicated in absence epilepsy, is sufficient to increase spike-wave seizures. We propose that activation of thalamic AMP-activated protein kinase, a sensor of cellular energetic stress and potentiator of metabotropic GABA<sub>B</sub>-receptor function, is a significant driver of hypoglycaemia-induced spike-wave seizures. We show that AMP-activated protein kinase augments postsynaptic GABA<sub>B</sub>-receptor-mediated currents in thalamocortical neurons and strengthens epileptiform network activity evoked in thalamic brain slices. Selective thalamic AMP-activated protein kinase activation also increases spike-wave seizures. Finally, systemic administration of metformin, an AMP-activated protein kinase agonist and common diabetes treatment, profoundly increased spike-wave seizures. These results advance the decades-old observation that glucose metabolism regulates thalamocortical circuit excitability by demonstrating that AMP-activated protein kinase and GABA<sub>B</sub>-receptor cooperativity is sufficient to provoke spike-wave seizures.

1 Department of Pharmacology, University of Virginia School of Medicine, Charlottesville, VA 22908, USA

2 Epilepsy Research Laboratory and Weil Institute for Neurosciences, Department of Neurological Surgery, University of California, San Francisco, San Francisco, CA 94143, USA

3 MD-PhD Program, Yale University School of Medicine, New Haven, CT 06520, USA

4 Department of Human Nutrition, Foods and Exercise, Virginia Polytechnic Institute and State University, Blacksburg, VA 24061, USA

5 The Robert M. Berne Center for Cardiovascular Research Center, University of Virginia School of Medicine, Charlottesville, VA 22908, USA

6 Department of Medicine, University of Virginia School of Medicine, Charlottesville, VA, USA

7 Department of Molecular Physiology and Biological Physics, University of Virginia School of Medicine, Charlottesville, VA 22908, USA

Correspondence to: Mark P. Beenhakker  
Department of Pharmacology  
University of Virginia School of Medicine  
Charlottesville, VA, 22908, USA  
E-mail: markbeen@virginia.edu

**Keywords:** epilepsy; metabolism; AMPK; GABA; thalamocortical

**Abbreviations:** AMPK = AMP kinase; ECoG = electrocorticogram; FRET = Förster resonance energy transfer; SWS = spike-wave seizure

## Introduction

Epilepsy is a disorder defined by spontaneously recurring seizures. Identifying factors that drive neural circuits to very rapidly, yet transiently, seize remains a major challenge. The genetic generalized epilepsies comprise one-third of all epilepsy syndromes and stem from complex, polygenic insults whose mechanisms remain poorly understood. Absence seizures are commonly observed in the genetic generalized epilepsies and appear as bursts of rhythmic, high amplitude spike-wave discharges that arise from synchronous activity among cortical and subcortical circuits.<sup>1–3</sup> Cortical structures are thought to initiate spike-wave seizures (SWSs), whereas thalamic structures serve as critical nodes for seizure generalization and maintenance.<sup>4–7</sup>

The brain consumes 20% of dietary glucose to sustain normal function.<sup>8</sup> Unsurprisingly, glucose availability has a considerable effect on seizures.<sup>9–12</sup> Over 80 years ago, Gibbs *et al.*<sup>13</sup> showed that hypoglycaemia precipitates seizures in children with absence epilepsy. Since then, we have learned that nearly 10% of patients diagnosed with early-onset childhood absence epilepsy are deficient in glucose transporter-1 (GLUT1),<sup>9,14</sup> the singular glucose transporter that shuttles glucose across the blood–brain barrier.<sup>15,16</sup> Hypoglycaemia-sensitive seizures are also observed in GLUT1 deficient mice<sup>17</sup> and a mouse model of SWS.<sup>11</sup> The cellular mechanisms that transduce glucose availability into SWS are unknown.

The conversion of cellular energy state into neural activity is complex.<sup>18,19</sup> The canonical transduction pathway involves the ATP-sensitive potassium ( $K_{ATP}$ ) channel. Largely regulated by ATP, the  $K_{ATP}$  channel adjusts the membrane voltage of the cell in response to cellular energy state; ATP depletion activates the channel, causing membrane voltage hyperpolarization.<sup>20,21</sup>  $K_{ATP}$  channels modulate neuronal activity in the hippocampus,<sup>22,23</sup> hypothalamus<sup>21,24</sup> and brainstem,<sup>25</sup> and are proposed to regulate limbic seizures.<sup>23,26</sup> Metabolic regulation of neural activity can also arise from the cooperative action between the metabotropic, B-type GABA receptor ( $GABA_B$ ) and the energy-sensitive AMP kinase (AMPK). During cellular stress, activated AMPK (p-AMPK) phosphorylates the  $GABA_B$ -receptor and potentiates  $GABA_B$ -receptor-mediated potassium currents.<sup>27</sup> Thalamocortical neurons are enriched in postsynaptic  $GABA_B$  receptors<sup>28</sup> and exert substantial control over thalamocortical oscillations and SWS.<sup>29–36</sup>

Here, we aimed to identify mechanisms that underlie hypoglycaemia-provoked SWS. We show that despite thalamocortical neuron expression,  $K_{ATP}$  channels play a minimal role in regulating thalamic neural activity during hypoglycaemia. We therefore tested the hypothesis that hypoglycaemia promotes functional coupling between AMPK and  $GABA_B$  receptors to provoke SWS. In support of this model, we demonstrate that AMPK activation strengthens  $GABA_B$ -receptor-associated currents in thalamocortical neurons and escalates thalamic network oscillations *in vitro*. Direct, thalamic AMPK activation also increases SWS. Metformin, a well-established diabetes treatment and AMPK activator, produced a profound increase in SWS that often progressed into lethal convulsive seizures. Collectively, we propose the first mechanistic framework to understand the long-established, clinical observation that low blood glucose exacerbates SWSs.

## Materials and methods

### Animals

All procedures followed the National Institutes of Health *Guide for Care and Use of Laboratory Animals* and were approved by the

University of Virginia Animal Care and Use Committee (Charlottesville, VA, USA). Unless otherwise stated, animals were housed at 23–25°C under an artificial 12-h light/dark cycle with food and water provided *ad libitum*. Wistar Albino Glaxo/from Rijswijk (WAG/Rij rats) were kindly provided by Dr Edward Bertram (University of Virginia). Non-epileptic Wistar IGS rats (stock no. 003) were purchased from Charles River. Wild-type DBA/2J mice (stock no. 000671) were purchased from The Jackson Laboratory. Both sexes were used in all experiments and no differences were observed. In total, 44 DBA/2J mice and 141 WAG/Rij rats were used.

### Simultaneous video-ECoG/EMG recordings

Rat electrocorticography (ECoG) devices were purchased from Plastics One. Mouse devices were assembled from parts purchased at Digikey. Stainless-steel recording electrodes were implanted bilaterally in the cortex while a reference electrode was placed in the cerebellum; EMG recordings were obtained from neck muscles. One week after surgery, animals were habituated to recording cages for 48 h. Filtered ECoG (0.3–100 Hz) and EMG (>100 Hz) signals were amplified with a model 3500 amplifier (A-M Systems) and sampled (200 Hz) with a PowerLab digitizer (ADI Instruments). All experiments occurred between Hours 2 and 10 of the 12-h dark cycle (*i.e.* Zeitgeber time 14–22). SWSs were scored manually by blinded individuals.

### Fasted blood measurements

In both rats and mice, tail vein blood was collected and glucose levels were measured with a human glucometer (Nova Max Plus, Nova Biomedical Corporation). Serum was separated from the same blood sample to quantify  $\beta$ -hydroxybutyrate levels using a colorimetric assay kit (Cayman Chemical, Item Number 700190).

### Insulin injection

Animals were injected intraperitoneally with either saline or insulin (3 IU/kg). Blood samples were collected in WAG/Rij rats 90 min before the start of the experiment, 90 min after injection and at experiment conclusion. Blood draws were not performed in mice during ECoG/EMG recordings due to elevated stress and casualty.

### Combined ECoG/EMG and drug infusion

A custom length guide cannula (Plastics One) was implanted in the left ventral basal nucleus of the thalamus (anterior-posterior –2.7 mm; medial-lateral –2.7 mm). Before experimentation, the dummy cannula was removed and replaced with a delivery cannula. Vehicle, 2-deoxyglucose [(2-DG); Millipore Sigma, Cat. no. D8375] or A-769662 (Tocris; Cat. no. 3336) solution was infused (50 nl/min) into the ventrobasal thalamus with a Microdialysis Syringe Pump (Harvard Apparatus).

### Lactate measurements

An incision in the leg of anaesthetized rats exposed the femoral artery, enabling the insertion of a catheter (Clay Adams) that was pushed towards the abdominal aorta. Arterial lactate blood samples were measured using an iSTAT instrument (Abbott Instruments).

## Immunohistochemistry

Anaesthetized animals were transcardially perfused with 4% paraformaldehyde in 0.1 M phosphate buffer (PB, pH 7.4). Then 40- $\mu$ m sections were cut from fixed brains with a Leica VT 1000S microtome (Leica Biosystems). All blocking and antibody solutions were prepared in an incubation buffer of 0.1% sodium azide and 2% normal goat serum. Primary antibody solutions containing rabbit anti-Kir6.2 (1:2000, Alomone Laboratories Cat. no. APC-020, RRID: AB\_2040124) and mouse anti-parvalbumin (1:2000, Sigma-Aldrich Cat. no. P3088, RRID: AB\_477329) were prepared and incubated for 2 days at 4°C. After PBS washes, sections were incubated overnight in secondary antibody solutions containing donkey anti-rabbit Cy3 (1:1000, Jackson ImmunoResearch Labs Cat. no. 711-165-152, RRID: AB\_2307443) and donkey anti-mouse AlexaFluor 488 (1:1000, Jackson ImmunoResearch Labs Cat. no. 715-545-151, RRID: AB\_2341099). Sections were imaged with a Z1 Axioimager (Zeiss Microscopy) and captured with consistent exposure settings.

## Quantitative PCR with reverse transcription

Here, 400- $\mu$ m brain sections were cut with a Leica VT 1200S microtome. Thalamus and somatosensory cortex were dissected and placed in sterile tubes containing RNAlater (Life Technologies). RNA was isolated using the RNAqueous 4PCR kit (Applied Biosystems) and/or RNAeasy mini kit (Qiagen) and DNase-treated. cDNA was prepared with the iScript cDNA Synthesis Kit (Bio-Rad) and PCR was used to assess levels of *Kcnj11* (Ensemble gene ID: ENSMUSG00000096146) mRNA expression using the PrimePCR™ Assay (Bio-Rad). The amplicon context sequence was designed to detect the Ensemble transcript ID: ENSMUST00000180081 (*Kcnj11*). Quantification of mRNA was performed with Sso Advanced™ SYBR® Green Supermix (Bio-Rad) that was compared to a standard curve generated by the PrimePCR™ Template for SYBR® Green. Only experiments with an  $R^2$  value  $\geq 0.95$  were included. *Kcnj11* transcript values were normalized to the control transcript provided by the PrimePCR™ Assay.

## Western blot analysis

Whole thalamus lysates were subjected to sodium dodecyl sulfate-polyacrylamide gel electrophoresis and transferred for 2 h onto nitrocellulose membranes<sup>37</sup> with antibodies (1:1000) against AMPK $\alpha$ 1/2 (C Cell Signaling Technology Cat. no. 2532, RRID: AB\_330331), p-AMPK $\alpha$ 1/2[T172] (Cell Signaling Technology Cat. no. 2535, RRID: AB\_331250) and *Gapdh* (Cell Signaling Technology Cat. no. 2118, RRID: AB\_561053CST). Goat anti-rabbit IR800 (LI-COR Biosciences Cat. no. 926-32211, RRID: AB\_621843 LICOR) served as the secondary antibody. Blots were scanned using Odyssey CLx infrared imaging system (LICOR). A common protein standard consisting of whole tissue lysate mixture of liver, heart and skeletal muscle was used to calculate phospho:total AMPK ratio.

## Acute slice preparation

Animals were transcardially perfused with an ice-cold protective recovery solution containing the following in (mM): 92 NMDG, 26 NaHCO<sub>3</sub>, 25 glucose, 20 HEPES, 10 MgSO<sub>4</sub>m, 5 Na-ascorbate, 3 Na-pyruvate, 2.5 KCl, 2 thiourea, 1.25 NaH<sub>2</sub>PO<sub>4</sub>, 0.5 CaCl<sub>2</sub>, titrated to a pH of 7.3–7.4 with HCl.<sup>38</sup> Horizontal slices containing the reticular thalamus and ventrobasal nucleus were cut with a Leica VT1200 vibratome and then kept at room temperature in oxygenated (95%

O<sub>2</sub>, 5% CO<sub>2</sub>) artificial CSF containing (in mM): 126 NaCl, 26 NaHCO<sub>3</sub>, 10 glucose, 2.5 KCl, 2 CaCl<sub>2</sub>, 1.25 NaH<sub>2</sub>PO<sub>4</sub>, 1 MgSO<sub>4</sub>.

## Patch-clamp recordings

Thalamic neuron recordings (31–33°C) were performed in 250- $\mu$ m slices visualized with a Zeiss Axio Examiner microscope and an ORCA Flash4.0 camera (Hamamatsu). Borosilicate glass recording electrodes were fabricated using a P1000 puller (Sutter Instruments). Whole-cell recording electrodes contained (in mM): 128 K-gluconate, 10 HEPES, 1 EGTA, 10 KCl, 1 MgCl<sub>2</sub>, 0.3 CaCl<sub>2</sub>, 0.3 Na-GTP, 2 ATP. Recordings were acquired using a Multiclamp 700B amplifier (Axon Instruments, Molecular Devices), low-pass filtered at 2 kHz and digitized at 10 kHz with a Digidata 1440A (Molecular Devices) and visualized with pClamp software (Molecular Devices). Data analyses were performed using custom code written in MATLAB (MathWorks, Natick, MA, USA). GABA<sub>B</sub>-receptor-activated K<sup>+</sup> currents were evoked by pressure ejection (Picospritzer, Parker Hannifin) 100  $\mu$ M baclofen (Millipore Sigma, Cat. no. B5399) adjacent to the soma of cells. To isolate these currents, kynurenic acid (1 mM, Millipore Sigma, Cat. no. K3375) and bicuculline methiodide (10  $\mu$ M; Tocris, Cat. no. 2503, Bio-Techne Corporation, RRID: SCR\_003689) were added to the artificial CSF. Internal solution included QX-314 (5  $\mu$ M, Tocris, Cat. no. 1014) to suppress action potentials. Only cells producing initially robust GABA<sub>B</sub>-mediated currents were examined so that response rundown could be measured. AMPK-activating drugs were dissolved in the internal pipette solution and included: metformin (Millipore Sigma, Cat. no. D150959), AMP (Millipore Sigma, Cat. no. A1752) and A-769662 (Tocris). To assess K<sub>ATP</sub> currents in ventrobasal nucleus neurons, glibenclamide (Abcam, Cat. no. ab120267) and/or diazoxide (Abcam, Cat. no. ab120266) was dissolved in the artificial CSF. Sucrose was added to low glucose-containing artificial CSF to compensate for osmolality changes.

## Extracellular multi-unit recordings

Network activity was recorded in 400  $\mu$ m thalamic slices within an interface chamber supplied with warm, oxygenated artificial CSF (31–33°C, 95% O<sub>2</sub>/5% CO<sub>2</sub>). Electrical stimuli were delivered to reticular thalamus with bipolar tungsten electrodes (FHC), while single tungsten electrodes placed in ventrobasal nucleus recorded extracellular activity. Filtered activity (0.1–3 kHz) was digitized and recorded with a Digidata 1440A and pClamp software. AMPK agonists and CGP-54626 (Tocris, Cat. no. 1088) were dissolved in the artificial CSF perfusate. Activity was quantified with custom MATLAB scripts.<sup>36</sup> Voltage amplitude thresholds were applied to detect action potentials and were set at 3–4 $\times$  the root mean square of the trace before stimulation. Oscillation duration was defined as the period between the stimulus onset and the last activity burst to occur within the specified inter-burst interval of 1 s.

## AMPKAR Förster resonance energy transfer imaging

We cloned AAV9-UPCamAMPKAR by moving the AMPKAR coding region from pPBbsr2-4031NES [a gift from Michiyuki Matsuda (Addgene\_105241)] into the plasmid pENN.AAV.CamKII0.4.eGFP.WPRE.rBG [a gift from James M. Wilson (RRID: Addgene\_105541)]. The insert was amplified by PCR using primers that added AgeI and BsrGI sites. The vector was digested with the same enzymes, thereby excising GFP and providing compatible restriction enzyme sites for the insert. Packaging in serotype AAV9 particles was performed by Vigene Biosciences (titre 3.58  $\times 10^{13}$  vg/ml). P14-P21 rats

received bilateral stereotaxic injection of AAV.Camk2a.AMPKAR.WPRE.Rbg targeted to somatosensory thalamus (300 nl per injection site). Acute thalamic brain slices (250  $\mu$ M) were prepared 2–4 weeks later and widefield imaged. Regions of interest were drawn in ImageJ and CFP/YFP signal intensities were measured using the FRETOffline plugin developed for ImageJ.<sup>39</sup>

## Experimental design and statistical analyses

Statistical analyses were performed in MATLAB. Data normality was tested using a combination of the Lilliefors test, the Anderson–Darling test and the Jarque–Bera test. Statistical details are described in the ‘Results’ section and corresponding [Supplementary material](#). Either parametric or non-parametric statistical analyses were performed, as indicated in the figure legends. A significance level was set at 0.05. Data are expressed as mean  $\pm$  SEM. Error bars reflect 95% confidence intervals.

## Data availability

The data that support the findings of this study are openly available in Dryad at <https://doi.org/10.5061/dryad.7pvmcvdsf>. Custom analysis code is available on GitHub at <https://github.com/blabuva>.

## Results

### Overnight fasting increases spike-wave seizures

Acute food withdrawal increases the number of spontaneous SWSs recorded in the DBA/2J strain of mouse.<sup>11</sup> We first confirmed this result ([Supplementary Fig. 1C–G](#)) and then determined if acute hypoglycaemia also provokes SWSs in the WAG/Rij rat, a long-standing, validated model of absence epilepsy.<sup>40,41</sup> We performed ECoG recordings in adult WAG/Rij rats for three consecutive days ([Fig. 1A](#)). Animals received food and water *ad libitum* for 2 days. On Day 3, animals fasted for 18 h, a duration required to achieve at least a 30% drop in blood glucose. We quantified SWSs during a 4-h period beginning at the same time of day for fed and fasted experiments. SWSs in WAG/Rij rats had an abrupt onset and occurred during behavioural arrest ([Fig. 1B](#)). Consistent with the efficacy of ethosuximide in treating human absence epilepsy, ethosuximide reduced SWSs in the rats ([Fig. 1C](#)). One hour before the fed and fasted recording sessions, we collected peripheral blood samples for blood glucose and serum ketone body (i.e.  $\beta$ -hydroxybutyrate) measurements. Ketone bodies represent an alternative fuel source for the brain during hypoglycemia<sup>42</sup> and are proposed to modulate seizures.<sup>43</sup>

Raster plots of individual SWSs ([Fig. 1D and E](#)) show that fasting increased SWSs relative to the fed state. Below each raster, we quantified the total number of SWSs per hour across the population; stacked histograms reveal the contribution of each animal to total SWS count for each 1-h-long bin. SWS count was nearly 2-fold higher during the fasted versus fed recording sessions for WAG/Rij rats ( $P=0.0078$ ,  $n=13$ ; [Fig. 1F](#)). Rats tested in the reverse order (i.e. fasted before fed) produced similar results ([Supplementary Fig. 2](#)). Seizure burden, measured as percentage duration seizing per recording session, was nearly 2-fold higher in WAG/Rij rats ( $P=0.00061$ ,  $n=13$ ; [Fig. 1H](#)) during fasted versus fed sessions. The increased seizure burden was largely driven by an elevated seizure count, not an increase in SWS duration ( $P=0.17$ ,  $n=13$ ; [Fig. 1G](#)).

Acute fasting elicited predictable changes in both blood glucose and  $\beta$ -hydroxybutyrate. Fasting decreased blood glucose

( $P=0.00097$ ,  $n=11$ ; [Fig. 1I](#)) and increased  $\beta$ -hydroxybutyrate ( $P=0.002$ ,  $n=11$ ; [Fig. 1J](#)), relative to the fed sessions. Fasting had similar effects on the DBA/2J mice ([Supplementary Fig. 1H–J](#)). We evaluated the correlation between SWS counts and glucose/ $\beta$ -hydroxybutyrate levels across both fed and fasted recording sessions. While correlation coefficients were not statistically significant, SWS count and  $\beta$ -hydroxybutyrate trended towards a positive correlation, whereas SWS count and blood glucose trended towards an inverse correlation ([Fig. 1K](#)). The observed trends suggested that either hypoglycaemia or ketosis—or both—might underlie the increase in SWS count following an acute fast.

### Elevated spike-wave seizure count associates with low glucose, not elevated ketone bodies

We next used a blunt manipulation—insulin injection—to disambiguate the effects of glucose and  $\beta$ -hydroxybutyrate on SWSs. In fed animals, insulin reduces blood sugar<sup>44,45</sup> without, presumably, affecting serum ketone bodies; although insulin can inhibit ketogenesis, this effect is primarily observed in fasted or diabetic animals.<sup>46,47</sup> We therefore tested the capacity of acute insulin administration in fed animals to reduce blood glucose and increase SWSs, without elevating serum  $\beta$ -hydroxybutyrate. We recorded SWSs in WAG/Rij rats during two 4-h recording sessions, each separated by a day of rest. One hour into the recording session, the animals received either insulin injection (3 IU, intraperitoneal) or volume-matched saline injection ([Fig. 2A](#)); we opted for a high insulin dose to induce a rapid and precipitous drop in glucose levels. We obtained peripheral blood samples 90 min after insulin injection to measure blood glucose and  $\beta$ -hydroxybutyrate ([Fig. 2A](#)). The 90-min time point aimed to capture the peak hypoglycaemic response induced by insulin.<sup>48</sup> SWS count, represented in stacked histograms, shows the contribution of each rat following either saline ([Fig. 2B](#)) or insulin ([Fig. 2C](#)) injection. To evaluate the effect of insulin on SWS count, we compared the mean number of SWSs observed during the 3 h following saline versus insulin injection. Relative to saline, insulin increased SWS count ( $P=0.036$ ,  $n=12$ ; [Fig. 2D](#)) and SWS burden in the rats ( $P=0.012$ ,  $n=12$ ; [Fig. 2F](#)); SWS duration was not affected ( $P=0.92$ ,  $n=12$ ; [Fig. 2E](#)). Rats tested in the reverse order (i.e. insulin before saline) produced similar results ([Supplementary Fig. 3](#)). Insulin injection produced a large reduction in blood glucose ( $P=0.0039$ ,  $n=9$ ; [Fig. 2G](#)), whereas  $\beta$ -hydroxybutyrate remained unchanged relative to saline injection ( $P=0.36$ ,  $n=9$ ; [Fig. 2H](#)).

We made similar observations for SWSs, blood glucose and  $\beta$ -hydroxybutyrate in DBA/2J mice ([Supplementary Fig. 4C–G](#)). As in [Fig. 1K](#), we evaluated the correlation between SWS count and glucose or  $\beta$ -hydroxybutyrate levels. This analysis revealed that SWS count and blood glucose were significantly and inversely correlated ( $R=-0.48$ ,  $P=0.046$ ), similar to the trend we observed during acute fasting (cf. [Fig. 2I](#) and [Fig. 1K](#)). As the inverse relationship between SWS count and blood glucose was consistent across fasting and insulin experiments, we concluded that hypoglycaemia is sufficient to increase SWSs.

### Intrathalamic 2-DG increases spike-wave seizures

Reduced peripheral blood glucose also reduces cerebral glucose.<sup>49</sup> Moreover, neural activity in the human thalamus, a structure critical for SWS generation, is particularly susceptible to moderate levels of acute hypoglycaemia.<sup>50</sup> Therefore, we tested the

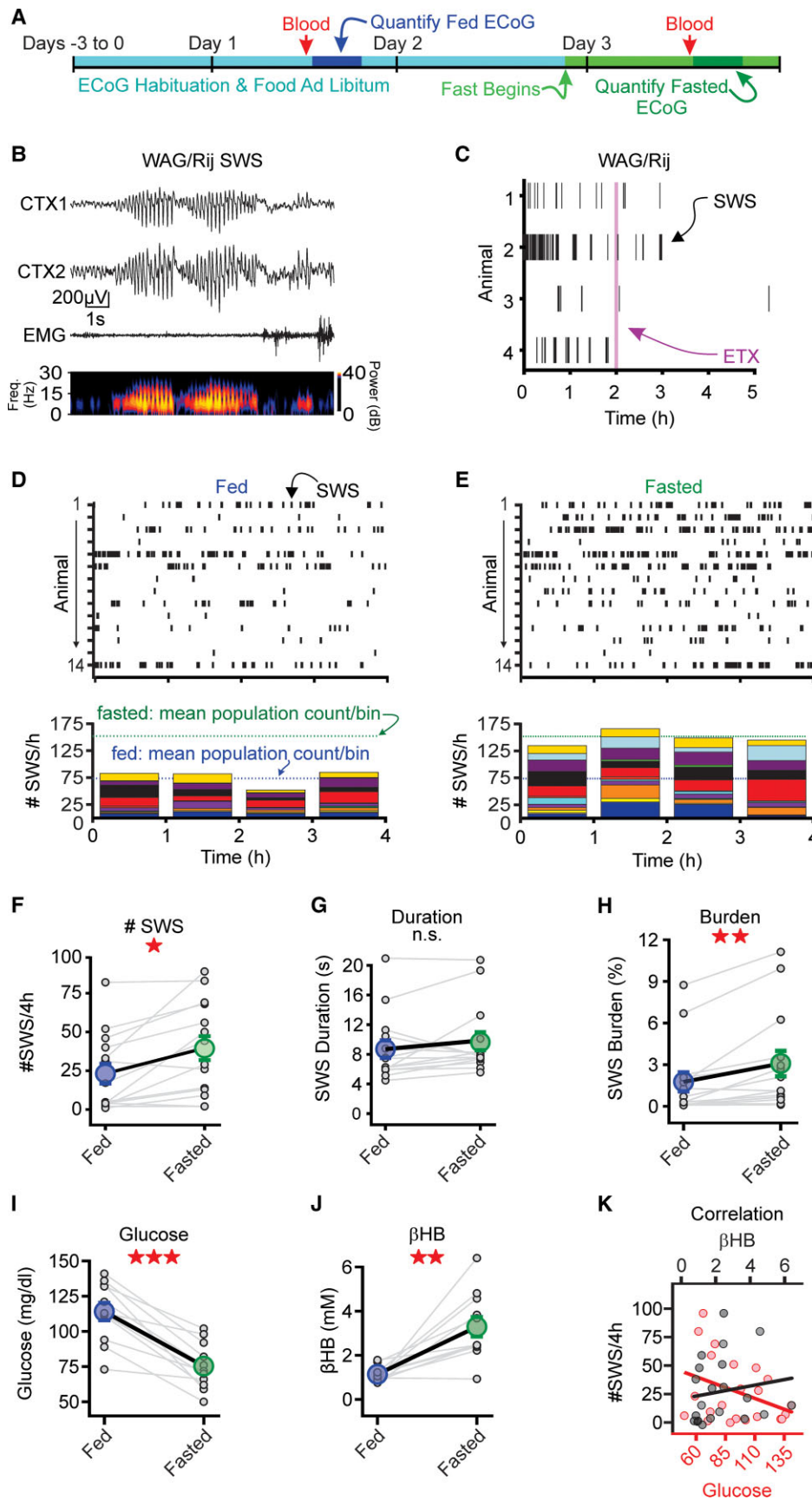


**Figure 1** Overnight fasting increases spike-and-wave discharges. (A) Seizure activity was evaluated for multiple days. Animals had access to food *ad libitum* before the overnight fast on Day 3. Before control and fasting experiments, blood was drawn for glucose and  $\beta$ -hydroxybutyrate ( $\beta$ HB) measurements. (B) Top: Continued

hypothesis that selective disruption of thalamic glycolysis is sufficient to provoke SWSs. We used a local drug delivery system to infuse 2-DG into the thalamus of WAG/Rij rats. 2-DG disrupts glycolysis by competing with native glucose as a substrate for glycolytic metabolism.<sup>51</sup> We targeted our local, unilateral 2-DG delivery to the somatosensory thalamus, a well-characterized SWS node,<sup>52</sup> while recording ECoG signals (Fig. 2J). After positioning a solution-filled cannula into the thalamus and recording basal activity for 3 h, we delivered either 2-DG (27  $\mu$ M)<sup>53</sup> or saline for an additional 3 h. Figure 2K shows the number of SWSs contributed by each animal to total SWS count per hour during intrathalamic infusion of saline or 2-DG. Comparing total SWS count during active delivery (i.e. pump turned on) showed that 2-DG infusion doubled SWS count, relative to saline ( $P = 0.010$ ,  $n = 9$ ; Fig. 2L). 2-DG did not affect SWS duration ( $P = 0.56$ ,  $n = 9$ ; Fig. 2M). Thus, targeted disruption of thalamic glycolysis is sufficient to provoke SWSs.

$K_{ATP}$  channels are well-characterized, glucose-sensitive ion channels<sup>21,24</sup> implicated in epilepsy.<sup>23,26</sup> Therefore, we determined whether thalamic neurons express  $K_{ATP}$  channels, and whether these channels confer glucose-sensitivity to thalamic neurons. Whereas immunohistochemical (Supplementary Fig. 5A and B), quantitative PCR (Supplementary Fig. 5C) and electrophysiological (Supplementary Fig. 5D) assays support the conclusion that thalamocortical neurons express  $K_{ATP}$  channels, low glucose challenges did not affect the intrinsic excitability of these neurons in either WAG/Rij rats (Supplementary Fig. 5H and I) or DBA/2J mice (Supplementary Fig. 5J and K), indicating that ion channel activity in thalamocortical neurons is unaffected during hypoglycaemic conditions. We therefore turned our attention to possible changes in synaptic properties induced by hypoglycaemia.

### Activated AMPK potentiates GABA<sub>B</sub>-receptor-mediated currents in the thalamus

AMPK serves as a master metabolic regulator<sup>54,55</sup> in many tissues, including brain,<sup>56–60</sup> by responding to the ratio of AMP or ADP to ATP within cells. As ATP levels drop, AMP or ADP activates AMPK, which is rapidly mobilized to restore the balance of cellular energy.<sup>55</sup> The kinase, therefore, functions specifically as a sensor of low levels of intracellular ATP and, more generally, as a sensor of energetic stress in the cell. Reliable cellular stressors that activate (i.e. phosphorylate) AMPK include hypoxia<sup>60,61</sup> and hypoglycaemia.<sup>56,62</sup> We first used western blots to determine whether AMPK activation is inducible in acute WAG/Rij rat, thalamic brain slices. We applied two indirect activators of AMPK, 2-DG and metformin, as well as the potent, direct activator A-769662, to thalamic slices and measured phosphorylated AMPK (p-AMPK) levels. Consistent with previous studies,<sup>63,64</sup> a 30-min bath application of 2-DG, metformin or A-769662 each produced a noticeable trend toward increased p-AMPK expression in a thalamic slice preparation, relative to a standard artificial CSF solution (Supplementary Fig. 6A and B). However, we also observed

significant differences in baseline p-AMPK signal across slices. As AMPK activation and deactivation are rapid signalling events, our variable p-AMPK signals probably reflect the challenge in mitigating the cellular stress imposed during thalamic tissue extraction. Consequently, we used a Förster resonance energy transfer (FRET)-based AMPK activity reporter, AMPKAR,<sup>64</sup> that allows within slice comparisons and offers better temporal resolution. Previous studies using AMPKAR show that AMPK activation occurs within 10–20 min following application of 2-DG, metformin or A-769662.<sup>63,64</sup> We generated a virally deliverable AMPK activity reporter driven by the excitatory neuron CaMKII promoter (Fig. 3A); thalamocortical neurons express CaMKII. AAV.Camk2a.AMPKAR.WPRE.Rbg was stereotactically delivered to the somatosensory nucleus of the thalamus of WAG/Rij rats. Following expression, we extracted acute brain slices containing the thalamus and measured AMPKAR FRET efficiency. Within 20 min, application of either metformin (10 mM;  $P = 0.0002$ ,  $n = 13$ ; Fig. 3B and C) or A-769662 (100 nM;  $P = 0.0129$ ,  $n = 10$ ; Fig. 3B and D) increased FRET efficiency relative to baseline, indicating elevated AMPK activity.

Next, we tested whether AMPK activation by metformin alters the intrinsic excitability of WAG/Rij rat thalamocortical neurons. We recorded individual thalamocortical neurons in the current clamp configuration while injecting a family of hyperpolarizing and depolarizing current steps (Supplementary Fig. 6C–E). Hyperpolarizing current injection was used to evaluate post-inhibitory rebound burst firing by thalamocortical neurons, a firing mode associated with SWSs.<sup>5</sup> Depolarizing current injection was used to evaluate general neuronal excitability. Rebound burst strength following a 2-s,  $-140$  pA, hyperpolarizing current injection was unaltered during 10 mM metformin application ( $P = 0.70$ ,  $n = 13$ ; Supplementary Fig. 6D). In contrast, 10 mM metformin produced a modest increase in excitability during depolarizing current injections [repeated-measures two-way ANOVA:  $F(1,245) = 15.3$ ,  $P = 0.0001$ ,  $n = 13$ ; Supplementary Fig. 6E]. The physiological relevance of the observed increase in spike count during a sustained, depolarizing current injection remains unclear as rebound burst firing mode, not tonic firing mode, is proposed to drive SWSs.<sup>5,65</sup>

AMPK-mediated enhancement of inhibitory GABA<sub>B</sub>-receptor signalling serves to curtail the damaging effects of ischaemia, a stressor that activates the kinase.<sup>27,61</sup> AMPK phosphorylates S783 of the R2, GABA<sub>B</sub>-receptor subunit that, in turn, potentiates receptor coupling to G-protein inwardly rectifying  $K^+$  channels (GIRKs).<sup>27,66</sup> The slow, long-lasting hyperpolarizing current that results from GIRK channel activation counters ischaemia-associated excitotoxicity.<sup>27</sup> As enhanced postsynaptic GABA<sub>B</sub>-receptor function increases SWS occurrence,<sup>29,67</sup> we proposed that hypoglycaemia-provoked SWSs rely on similar AMPK-GABA<sub>B</sub>-receptor cooperativity during energetic stress.

We evaluated the effects of AMPK on postsynaptic GABA<sub>B</sub>-receptor function by manipulating the internal pipette solution of

#### Figure 1 Continued

Representative SWS from a WAG/Rij rat (right). CTX1 and CTX2 are cortical ECoG recordings while EMG recording is from the neck. EMG activity was suppressed during the SWS, corresponding to behavioural arrest. Bottom: Spectrograms from CTX1 showing increased power in the 5–8 Hz frequency band during the SWS. (C) Ethosuximide (ETX; 200 mg/kg) suppressed SWSs in the WAG/Rij rat. Purple line indicates intraperitoneal injection of ETX. (D and E) Top: SWS rasters during fed (D) and fasted (E) conditions in rats ( $n = 13$ ). Bottom: Stacked histograms showing hourly SWS count for each rat during fed and fasted conditions. Blue and green dashed lines represent mean of the total SWS count per bin during fed and fasted conditions, respectively. (F–H) Fasting increased SWS count, duration and burden. (I and J) Fasting decreased blood glucose and increased  $\beta$ -hydroxybutyrate, relative to the fed state ( $n = 11$ ). (K) Blood glucose (red) or serum  $\beta$ -hydroxybutyrate (black) versus SWS count. For each panel, small circles represent data from one animal, while large circles represent the sample mean ( $\pm$  SE). \* $P < 0.05$ , \*\* $P < 0.01$ , \*\*\* $P < 0.001$ , not significant (n.s.) from the Wilcoxon sign rank test. See Supplementary Table 1 for details.

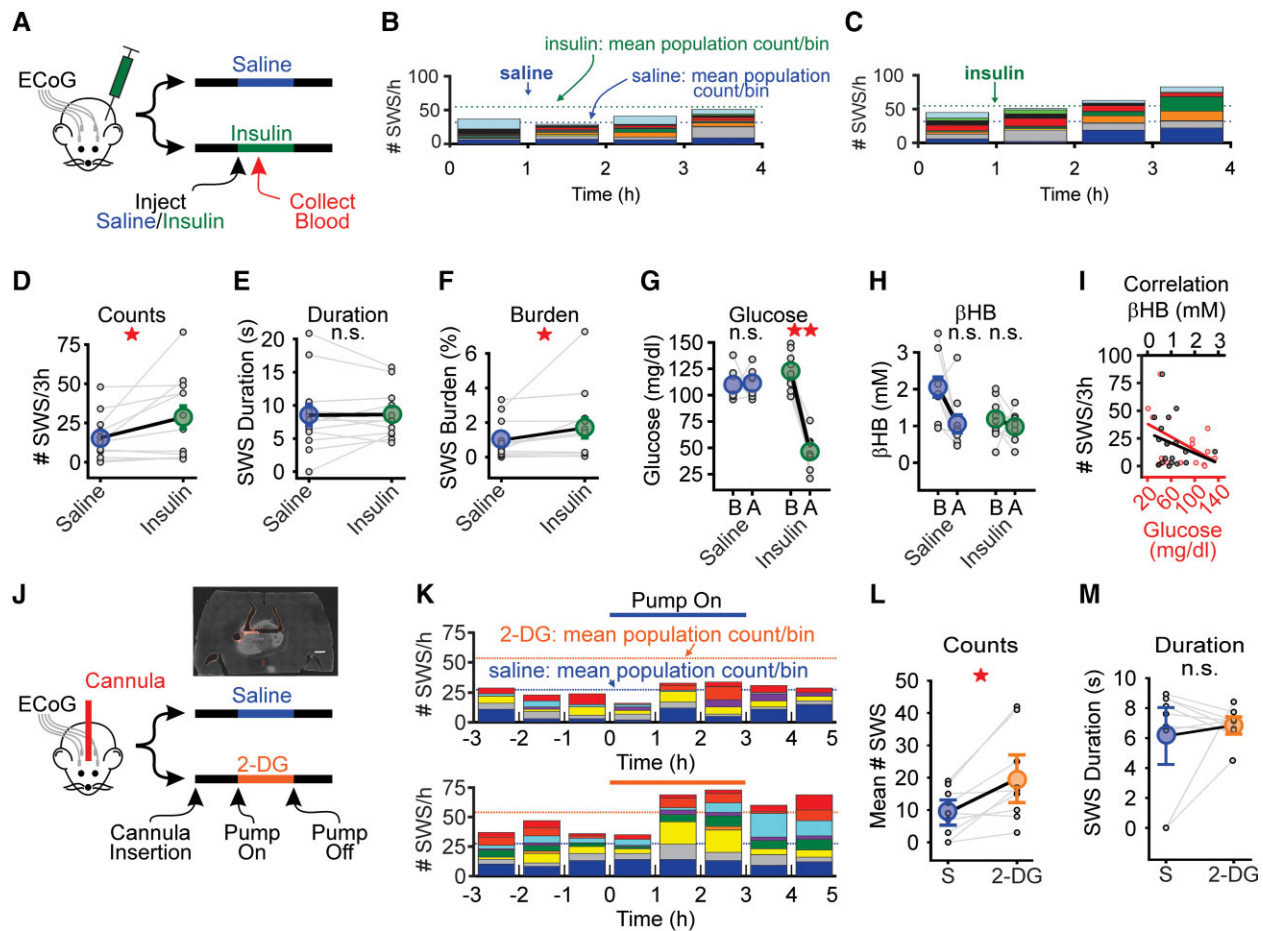


**Figure 2** Elevated SWS count tracks with low blood glucose. (A) Animals received either saline or insulin (3 IUs) 1 h into a 4-h recording session ( $n = 12$ ). Blood was collected at 90 min post-injection for glucose and serum  $\beta$ -hydroxybutyrate ( $\beta$ HB) analysis. (B and C) Stacked histograms showing SWS counts for WAG/Rij rats after saline (B) or insulin (C) injection. Blue dashed lines represent the mean total SWS count per bin after saline. Green dashed lines represent the mean total SWS count per bin after insulin. (D–F) Insulin increased mean SWS count and burden, but not duration, relative to saline injection. If an animal did not have SWSs, then duration was defined as zero. (G and H) In rats, insulin significantly decreased blood glucose but had no effect on serum  $\beta$ -hydroxybutyrate concentration. B = before injection; A = after injection. (I) Plot comparing SWS count to blood glucose (red) and serum  $\beta$ -hydroxybutyrate (black) in rats ( $n = 9$ ). (J) Rats implanted with ECoG electrodes and unilateral cannulae in somatosensory thalamus received either saline or 2-DG on separate days. Pump was automatically turned on after a 4-h baseline recording and turned off 3 h later. Inset shows example of cannula placement in thalamus. A 100- $\mu$ m horizontal section from rat following injection of Dil (scale = 1 mm). (K) Stacked histograms showing SWS count per hour for saline infusion (top) and 2-DG (bottom). Blue and orange dotted lines represent the mean of the total SWS count per bin during the infusion of saline and 2-DG, respectively. (L and M) 2-DG infusion increased mean SWS count during the infusion period (i.e. 0–3 h) whereas duration was unaffected. In each panel, small circles represent data from one animal, whereas large circles represent the sample mean ( $\pm$  SE). \* $P < 0.05$ , \*\* $P < 0.01$ , not significant (n.s.) from Wilcoxon sign rank test or paired t-test. See [Supplementary Table 2](#) for details.

voltage-clamped neurons recorded in the whole-cell patch-clamp configuration. We evoked  $GABA_B$ -receptor-mediated GIRK currents in WAG/Rij thalamocortical neurons by pressure ejection of the  $GABA_B$ -receptor agonist baclofen (100  $\mu$ M, 5 ms) proximal to the recorded neuron every 3 min (Fig. 3E). Similar to observations made in cultured hippocampal neurons,<sup>27</sup> successive baclofen applications produced progressively smaller responses in thalamocortical neurons recorded under control conditions (i.e. internal solution containing 2 mM ATP; Fig. 3F–H, black), a response rundown attributed to cell surface instability of the receptor.<sup>27,68</sup> AMPK activation in cultured hippocampal neurons increases cell surface  $GABA_B$ -receptor stability and counteracts baclofen response rundown.<sup>27,68</sup> Similarly, when included in the internal pipette solution of recorded thalamocortical neurons, AMPK activators metformin<sup>69</sup> and A-769662<sup>70</sup> eliminated rundown to repeated baclofen application (Fig. 3G and H, red); inclusion of AMP produced a non-significant trend of this rundown elimination (Fig. 3F). We quantified these observations by normalizing the

amplitude of all baclofen responses to the amplitude of the first baclofen response. Thus, under control conditions, baclofen-activated GIRK currents exhibited rundown, relative to starting responses, while inclusion of AMP in the recording pipette produced responses that trended larger [repeated-measures two-way ANOVA:  $F(5,65) = 2.21$ ,  $P = 0.06$ ; Fig. 3F]. Rundown was significantly mitigated when 1 mM metformin [repeated-measures two-way ANOVA:  $F(5,75) = 2.79$ ,  $P = 0.022$ ; Fig. 3G] or 100 nM A-769662 [repeated-measures two-way ANOVA:  $F(5,65) = 2.83$ ,  $P = 0.022$ ; Fig. 3H] was added to the internal pipette solution. Thus, AMPK activation potentiates postsynaptic  $GABA_B$ -receptor-mediated GIRK currents in thalamocortical neurons.

### AMPK agonists intensify $GABA_B$ -receptor-dependent epileptiform oscillations

We next tested whether thalamic circuit oscillations recorded *in vitro* are also sensitive to AMPK activation. Electrical stimulation of



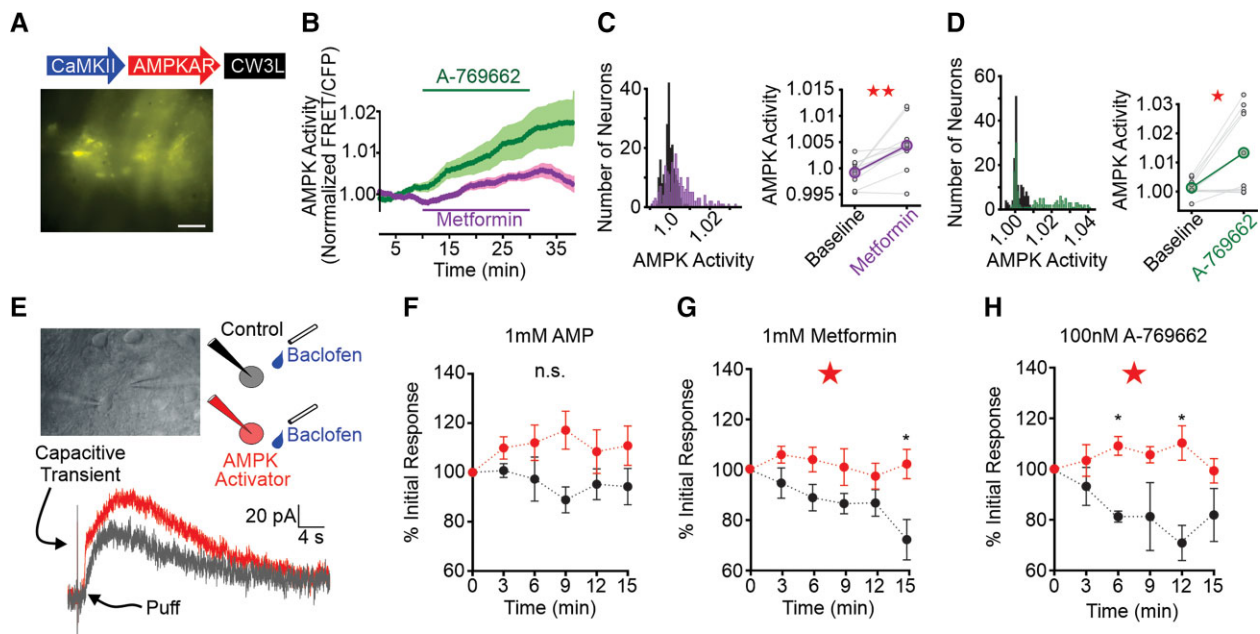


**Figure 3** Thalamocortical neuron AMPKAR expression and GIRK currents following AMPK activation. (A) Thalamocortical neuron AMPKAR expression based on construct developed by Tsou et al.<sup>63</sup> and Konagaya et al.<sup>64</sup> Scale bar = 50  $\mu$ m. (B) Thalamocortical neuron AMPKAR FRET efficiency increased during application of metformin (10 mM, purple), A-769662 (100 nM, green). FRET values are normalized to the 3-min baseline period prior to drug application. (C) Histogram (left) of FRET values for all neurons during baseline (black) and metformin (purple) application. Pairwise comparison (right) of mean FRET per slice in baseline and metformin application. (D) Histogram of FRET values (left) and mean pairwise comparisons (right) for A-769662 application. See [Supplementary Table 3](#) for data values. (E) Top left: Whole-cell patch-clamp recording in an acute thalamic brain slice. Baclofen application pipette is on the right. Top right: Schematic of experiment. Whole-cell patch-clamp recordings were performed using recording pipettes containing either control internal solution (black) or internal solution supplemented with an AMPK activator (red). A second pipette, placed proximal to the patched neuron, contained 100  $\mu$ M baclofen (blue). Bottom: Representative traces of evoked GABA<sub>B</sub> currents with recording pipette containing AMPK activator (grey, t = 3 min; red, t = 9 min). Arrows point to capacitive transient of a voltage-step used to measure access resistance and puff onset. (F) AMP (1 mM) stabilized, but did not significantly mitigate ( $P = 0.06$ ), GABA<sub>B</sub>-receptor current rundown. (G) Metformin (1 mM) significantly prevented GABA<sub>B</sub> current rundown relative to control. (H) A-769662 (100 nM) similarly attenuated GABA<sub>B</sub> current rundown relative to control. For F–H, response amplitude of GABA<sub>B</sub>-receptor mediated K<sup>+</sup> current was normalized to the current amplitude at 3 min (t = 1); data are mean  $\pm$  SE; \* $P < 0.05$ . Repeated-measures two-way ANOVA; unpaired t-test for pairwise comparison. See [Supplementary Table 3](#) for details.

corticothalamic afferents in acute brain slices containing somatosensory thalamus is a well-established model of both sleep spindles and SWSs<sup>71–73</sup> and provides a measure of thalamic circuit excitability. Several studies demonstrate that spindle-like activity evoked in the thalamic slice preparation relies on A-type GABA (GABA<sub>A</sub>) receptor-mediated signalling, whereas SWS-associated epileptiform activity relies on robust activation of GABA<sub>B</sub> receptors expressed by thalamocortical neurons.<sup>30,34,35</sup> Using this model, we tested the sensitivity of both GABA<sub>B</sub>-receptor-dependent and -independent activity to AMPK activation.

Pilot studies suggested that 10  $\mu$ M A-769662 potentiates evoked oscillations generated in slices wherein GABA<sub>A</sub> and GABA<sub>B</sub> receptors are both functional ([Supplementary Fig. 7A](#)). Next, to dissect the contribution of GABA<sub>A</sub> and GABA<sub>B</sub> receptors to this effect, we evoked thalamic, SWS-like oscillations in WAG/Rij brain slices by stimulating neurons of the reticular thalamic nucleus in the presence of the GABA<sub>A</sub> receptor antagonist, bicuculline (10  $\mu$ M; [Fig. 4A and B](#)). Oscillations were evoked once per minute and action potential activity was recorded with extracellular field electrodes placed within somatosensory thalamus. In the absence of any additional pharmacological manipulations, oscillations evoked during bicuculline application are generally stable<sup>36</sup> but can exhibit some rundown<sup>74</sup> ([Supplementary Fig. 7B](#)). Following a baseline period wherein oscillations were evoked in 10  $\mu$ M bicuculline, we co-applied either metformin (5 mM) or A-769662 (10  $\mu$ M) to the

perfusate for 40 min, followed by a 20-min washout period. Both metformin ([Fig. 4C](#)) and A-769662 ([Fig. 4G](#)) prolonged evoked oscillations. Plotting binned spikes in a greyscale heat map showed that oscillation prolongation occurred within 10 min of metformin ([Fig. 4D](#)) or A-769662 ([Fig. 4H](#)) application. Such was also the case when pooling all slice experiments and tracking oscillation duration across time (metformin: [Fig. 4E](#); A-769662: [Fig. 4I](#)). The pooled data showed that oscillation duration increased by 20% during metformin application ( $P = 0.0027$ ,  $n = 11$ ; [Fig. 4F](#)) and 12% during A-769662 application ( $P = 0.0082$ ,  $n = 15$ ; [Fig. 4J](#)). These results indicate that AMPK-GABA<sub>B</sub> cooperativity modulates thalamic oscillations.

We also evaluated the sensitivity of evoked network activity during AMPK activation when GABA<sub>B</sub>, not GABA<sub>A</sub>, receptors were blocked. GABA<sub>B</sub>-receptor blockade produces oscillations that are disorganized and short in duration.<sup>34,35</sup> Nonetheless, activity evoked during GABA<sub>B</sub>-receptor blockade provides an opportunity to evaluate the sensitivity of thalamic circuits to AMPK activity in the absence of GABA<sub>B</sub>-receptor activity. We recorded thalamic network activity in the presence of 20 nM CGP-54626, a potent GABA<sub>B</sub>-receptor blocker,<sup>75</sup> using the same stimulation paradigm described previously. As expected, evoked activity was less oscillatory and shorter in duration, relative to oscillations evoked during GABA<sub>A</sub> receptor blockade (cf [Fig. 4K and Fig. 4C and G](#)). Importantly, application of the potent, direct AMPK activator

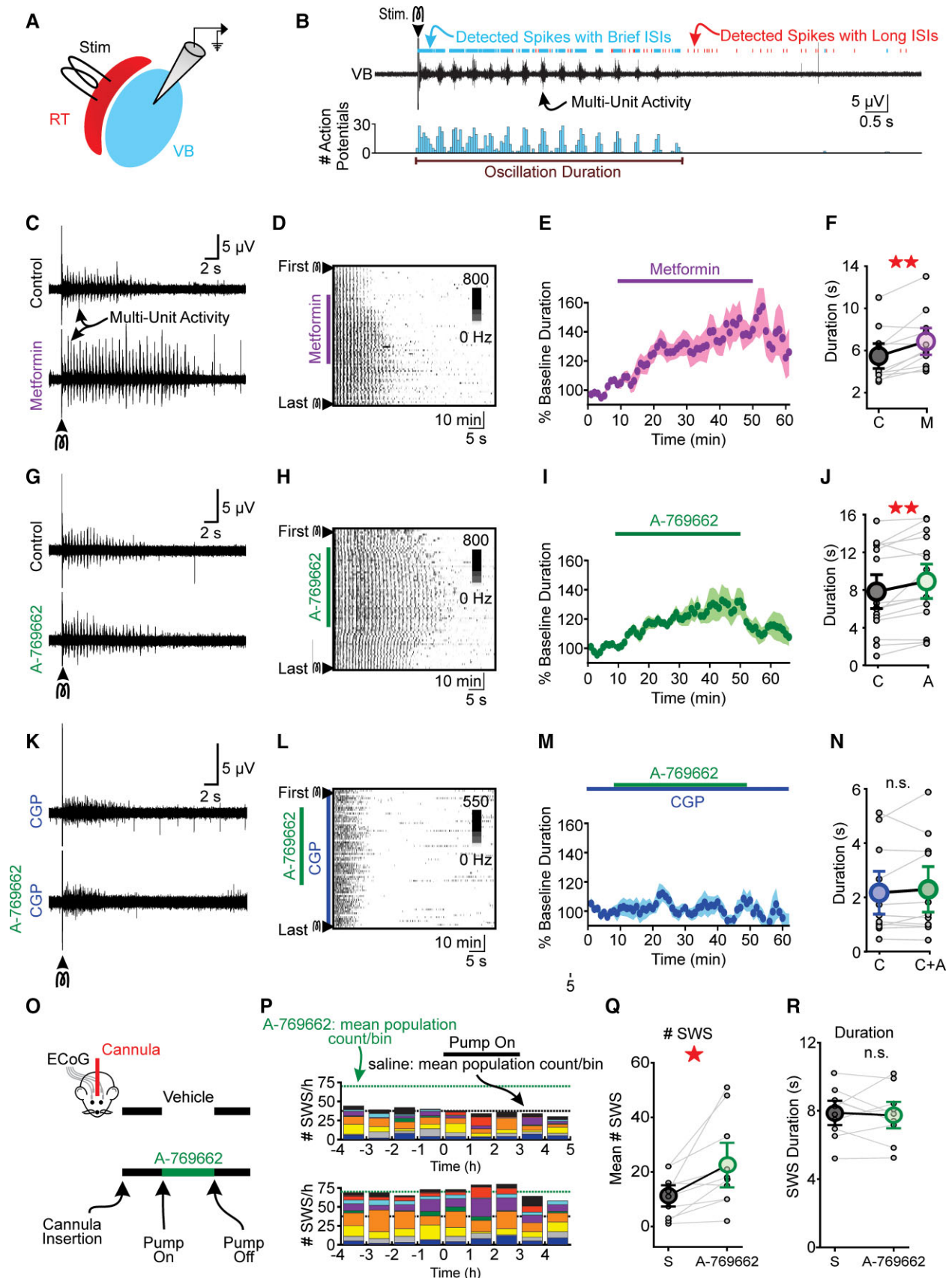


**Figure 4** AMPK activators intensify thalamocortical oscillations *in vitro* and SWS *in vivo*. (A) Thalamocortical oscillations were electrically evoked in acute brain slices containing reticular thalamus (RT) and ventrobasal nucleus (VB) thalamus. (B) Top: A single stimulus evoked seconds-long bursting activity in ventrobasal nucleus that was evaluated by measuring interspike intervals (see ‘Materials and methods’ section). Bottom: Histogram of detected spikes. Bin size = 100 ms. (C) Representative oscillations and (D) spike raster during control and 5 mM metformin. Oscillations were evoked Continued

A-769662 did not affect activity duration ( $P=0.43$ ,  $n=11$ ; Fig. 4K–N). Thus, prolongation of oscillations evoked in the acute thalamic slice requires functional GABA<sub>B</sub> receptors.

The observation that AMPK activation specifically modulated SWS-like activity in the WAG/Rij rat thalamic slice motivated us to determine whether A-769662 is sufficient to provoke SWSs recorded *in vivo*. We compared the actions of saline and 10  $\mu\text{M}$  A-769662 on SWS occurrence in cannulated (somatosensory thalamus, unilateral) WAG/Rij rats (Fig. 4O). Figure 4P shows the contribution of each rat to total SWS count per hour before, during and after intrathalamic infusion of saline or A-769662. Several rats produced an unusually high number of SWSs before pump activation, an effect that possibly reflects passive diffusion of the potent AMPK activator. Nonetheless, relative to saline infusion, A-769662 infusion produced more SWSs ( $P=0.017$ ,  $n=10$ ; Fig. 4Q), but did not change SWS duration ( $P=0.72$ ,  $n=10$ ; Fig. 4R). These data demonstrate that like fasting (Fig. 1), insulin injection (Fig. 2B–F) and thalamic 2-DG infusion (Fig. 2K–M), thalamic AMPK activation is sufficient to increase SWSs in WAG/Rij rats.

### Metformin increases spike-wave seizures and causes status epilepticus in WAG/Rij rats

Similar to A-769662, metformin potentiated postsynaptic GABA<sub>B</sub>-receptor function in thalamocortical neurons and strengthened SWS-like oscillations. We therefore hypothesized that metformin would also exacerbate SWSs. To test this hypothesis, we administered metformin systemically (intraperitoneal) to WAG/Rij rats and monitored SWSs. We delivered metformin systemically as this route is more comparable to its oral administration in patients. We tested metformin at 150 and 200 mg/kg, two doses used in previous rat studies.<sup>76–78</sup> While the lower dose of metformin produced a trend towards increased SWSs (see next), WAG/Rij rats injected with 200 mg/kg metformin advanced through a stereotyped progression of worsening seizure phenotype. Within 20 min of 200 mg/kg metformin injection, SWS count increased by several-fold and the rats quickly entered a state of nearly continuous SWSs for 30 min (i.e. absence status epilepticus, Fig. 5A). Within 70 min of metformin injection, all animals experienced generalized tonic-clonic seizures (convulsive status epilepticus, Fig. 5A) for ~20 min, after which five of six animals died. The one surviving rat remained in convulsive status epilepticus for 11 h before seizures subsided. Figure 5B shows binned SWS counts for baseline (i.e. no injection) and saline injection, whereas Fig. 5C shows SWS counts before/after 150 and 200 mg/kg metformin injections, respectively. Binned SWS counts for non-epileptic Wistar rats, the strain of rat from which WAG/Rij rats are derived,<sup>79</sup> are shown in Fig. 5D and E.

We compared the total SWS count for each animal during the 2 h following saline versus metformin injection (Fig. 5F and G). WAG/Rij rats injected with 200 mg/kg metformin produced more SWSs, relative

to saline ( $P=0.036$ ,  $n=6$ ; Fig. 5F). The 200 mg/kg metformin did not provoke seizures in non-epileptic Wistar rats (Fig. 5G) and 150 mg/kg metformin produced a trend towards increased SWSs in WAG/Rij rats ( $P=0.22$ ,  $n=6$ ; Supplementary Fig. 8B) relative to saline. In Wistar rats, 150 mg/kg metformin did not affect SWS count (Supplementary Fig. 8E).

At high doses, metformin causes lactic acidosis.<sup>80</sup> Therefore, we measured blood lactate after metformin/saline injection in a separate cohort of WAG/Rij and Wistar rats. The 1-h time point aligned with the pronounced change in SWSs and the emergence of tonic-clonic seizures in the WAG/Rij rat. Lactate did not increase in WAG/Rij rats injected with 150 mg/kg metformin ( $P=0.16$ ,  $n=7$ ; Supplementary Fig. 8C). After 200 mg/kg injection, we observed a 3-fold increase in lactate ( $P=0.016$ ;  $n=7$ ; Fig. 5F) and all rats perished within 1 h. The 200 mg/kg metformin also increased lactate in Wistar rats ( $P=0.03$ ;  $n=5$ ; Fig. 5G). Post-metformin lactate levels in WAG/Rij and Wistar rats were similar ( $P=0.64$ ).

As the WAG/Rij seizure response to lactate-producing doses of metformin is complex, we speculate that lactate's actions on WAG/Rij neural circuits are likewise complex. Nonetheless, we tested whether GABA<sub>B</sub>-receptor-dependent oscillations evoked in acute thalamic slices from WAG/Rij rats were sensitive to activation of HCAR1, a receptor for lactate that, like AMPK, has recently been shown to augment GABA<sub>B</sub>-receptor function.<sup>81</sup> 3Cl-5OH-BA, a selective HCAR1 receptor agonist, prolonged evoked oscillations by 40% ( $P=0.025$ ,  $n=4$ ; Fig. 5H and I). Thus, both p-AMPK and lactate are sufficient to augment GABA<sub>B</sub>-receptor function and exacerbate thalamic network oscillations associated with SWSs. However, it remains formally possible that p-AMPK actions on GABA<sub>B</sub>-receptor function are indirect, resulting from its ability to elevate lactate.

## Discussion

Here, we first advance the observation that hypoglycaemia provokes SWS by showing that selective blockade of thalamic glycolysis in the WAG/Rij rat is sufficient to provoke SWS. Specifically, we show that hypoglycaemia probably activates AMPK in the thalamus, and that activated AMPK augments postsynaptic GABA<sub>B</sub>-receptor signalling in thalamocortical neurons. AMPK-GABA<sub>B</sub>-receptor enhancement strengthens epileptiform, GABA<sub>B</sub>-receptor-dependent oscillations in acute thalamic slices and elevates SWS *in vivo*. Last, we report that metformin, a common diabetes treatment and AMPK activator,<sup>82</sup> powerfully instigates SWS in the WAG/Rij rat. These findings provide the first molecular framework for understanding how glucose availability regulates generalized SWS.

### Hypoglycaemia and spike-wave seizures

Glucose fuels the brain and is the most robust energy source for generating ATP. Moreover, glucose-derived metabolites are

#### Figure 4 Continued

once every 60 s in the presence of bicuculline. (E) Normalized oscillation duration versus time for all metformin experiments. Durations were normalized to baseline values per slice. (F) Co-application of metformin increased oscillation duration relative to baseline. (G) Representative oscillations and (H) spike raster during control (bicuculline) and 10  $\mu\text{M}$  A-769662 co-application. (I) Normalized oscillation duration versus time for all A-769662 experiments. (J) A-769662 increased oscillation duration relative to baseline. (K) Representative oscillations and (L) spike raster during control (20 nM CGP-54626) and 20 nM CGP-54626 + 10  $\mu\text{M}$  A-769662. Blocking GABA<sub>B</sub> receptors with CGP resulted in briefer and more disorganized spiking activity. (M) Normalized oscillation duration versus time for all CGP experiments. (N) Mean duration of evoked activity was not different between CGP-54626 and CGP-54626 + A-769662 co-application. (O) Direct infusion of A-769662 in somatosensory thalamus increased SWSs. WAG/Rij rats implanted with ECoG electrodes and unilateral cannulae in somatosensory thalamus received either saline or 10  $\mu\text{M}$  A-769662 for 3-h on separate days. (P) Stacked histograms showing SWS counts for each animal [saline (*top*) and A-769662 (*bottom*)]. Black and green dotted lines represent mean of the total SWS count per bin after infusion start for saline and A-769662, respectively. (Q) A-769662 infusion increased mean SWS count during the infusion period (i.e. 0–3 h) but not (R) SWS duration. All data are represented as mean  $\pm$  SE. \* $P < 0.05$ , \*\* $P < 0.01$ , not significant (n.s.) from paired student's t-test or Wilcoxon sign rank test. Each circle in the figure represents one slice (C–N) or animal (Q–R). See Supplementary Table 4 for details.

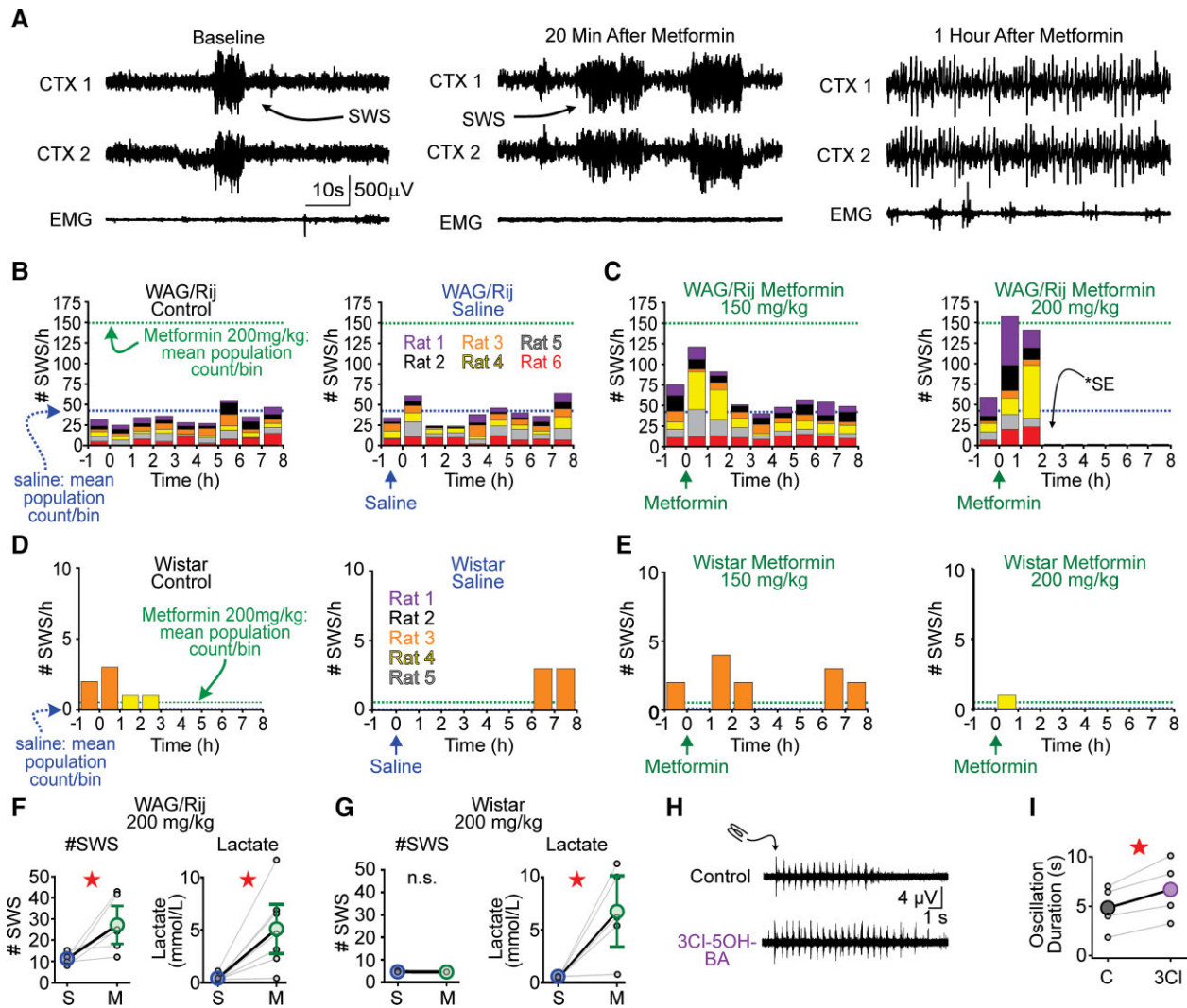


**Figure 5** Metformin elevates SWSs and can cause status epilepticus in WAG/Rij rats. (A) Representative recording of WAG/Rij rat injected with 200 mg/kg metformin. Left: ECoG/EMG activity before metformin injection. Arrow indicates spontaneous SWS. Middle: At 20 min after metformin injection, SWSs occurred frequently and marked the beginning of continual SWSs. Right: ECoG/EMG recording 1 h after metformin injection, wherein the transition from SWSs to convulsive status epilepticus (SE) has occurred. Heightened muscle activity is recorded in the EMG, consistent with motor activity induced by tonic-clonic seizures. (B) WAG/Rij rat SWS counts for control and saline. (C) SWS counts in same WAG/Rij rats after 150 mg/kg and 200 mg/kg metformin. Stacked histograms showing SWS counts per animal for all conditions. Dotted lines indicate the mean of the total SWS count per bin following saline (blue) and 200 mg/kg metformin (green) injection, respectively. (D) Non-epileptic Wistar rat SWS counts for control and saline. (E) Wistar rat SWS counts in stacked histogram format for 150 and 200 mg/kg metformin. (F) Injection with 200 mg/kg metformin increased WAG/Rij SWS counts, while lactate (mmol/l) levels trended higher. (G) Injection with 200 mg/kg metformin did not evoke any seizure activity in Wistar rats despite comparable changes in lactate (mmol/l). (H) Representative multi-unit recordings of evoked thalamocortical oscillations in ventrobasal nucleus (VB) thalamus following electrical stimulation of reticular thalamus (RT). Top: Control trace showing oscillation evoked during baseline conditions. Bottom: Oscillation evoked during 3CI-5OH-BA application. (I) 3CI-5OH-BA significantly prolonged the duration of evoked oscillations. In each panel, data are presented as mean  $\pm$  SE. Each dot represents one animal (F and G) or slice (I). \* $P < 0.05$  or not significant (n.s.) from paired, t-test or Wilcoxon sign rank pairwise comparison. See [Supplementary Table 5](#) for details.

required for the synthesis of several neurotransmitters that regulate neuronal excitability, including glutamate and GABA.<sup>18,83</sup> SWS exacerbation by hypoglycaemia was first reported nearly 80 years ago,<sup>13</sup> and impaired glucose handling continues to associate with the genetic generalized epilepsies today. Mutations in *SLC2A1*, the gene encoding GLUT1, are found in 1% of all genetic generalized epilepsy patients and specifically account for 10% of early-onset childhood absence epilepsies.<sup>9</sup> Moreover, nearly half of GLUT1 deficient patients produce 2.5–4 Hz spike-wave discharges,<sup>14</sup> electrographic patterns similar to SWS associated with the absence epilepsies. The *SLC2A1* mutation impairs glucose

transport across the blood–brain barrier. As GLUT1-deficient patients present with CSF containing  $<60$  mg/dl glucose,<sup>84</sup> these patients lack the necessary cerebral glucose to maintain proper brain function.

An effective therapy for GLUT1 deficiency syndrome is the ketogenic diet,<sup>85</sup> a high-fat, low carbohydrate diet that switches the body's fuel source from glucose to ketone bodies.<sup>86</sup> As the brain shifts towards a reliance on ketone bodies for fuel, a change that takes several days, seizures in GLUT1 patients on the diet eventually abate. Indeed, the anti-convulsant effects of the ketogenic diet extend well beyond GLUT1 deficiency.<sup>43,87–89</sup> Several studies

specifically attribute the anti-seizure effects of the diet to elevated ketone bodies.<sup>89–91</sup> And yet, here we report that acute fasting—a manipulation that elevates ketone bodies—exacerbates SWS. We speculate that during acute hypoglycaemia, the pro-SWS actions of hypoglycaemia outweigh the anti-SWS mechanisms of ketosis, if any, to provoke SWS; notably, the diet is considered only moderately effective in treating the absence epilepsies.<sup>92,93</sup> If true, then evaluating whether absence seizure occurrence in patients correlates with normal, diurnal fluctuations in blood glucose may ultimately provide novel insights into improving seizure control.

Curiously, our observations that hypoglycaemia, 2-DG and metformin can aggravate absence seizures appear to contradict the proposed, seizure-suppressing use of these drugs. Indeed, both 2-DG<sup>94,95</sup> and metformin<sup>76</sup> show great promise in treating temporal lobe seizures. However, both 2-DG and metformin may ultimately belong to a sizeable list of anti-seizure drugs that counterintuitively worsen absence epilepsy. Drugs in this list—carbamazepine, oxcarbazepine, phenytoin, vigabatrin and tiagabine—are used to treat temporal lobe seizures and yet aggravate absence seizures.<sup>96–103</sup> Indeed, both vigabatrin<sup>98</sup> and tiagabine<sup>104</sup> can induce absence status epilepticus, a state of continuous and prolonged SWS and the EEG pattern we observed in WAG/Rij rats following a high metformin dose. Both vigabatrin and tiagabine increase the availability of extracellular GABA and are hypothesized to exacerbate absence seizures by promoting GABA<sub>B</sub>-receptor activation.<sup>36,75,97</sup> Thus, the finding that 2-DG and metformin may in fact both reduce temporal lobe seizures and aggravate absence seizures may ultimately align with our current understanding of some anti-seizure drugs.

### GABA<sub>B</sub>-receptor mediated inhibition in the thalamus

Our results support the hypothesis that energetic stress activates thalamic AMPK that, in turn, upregulates GABA<sub>B</sub>-receptor function. Promoting GABA<sub>B</sub>-receptor function elevates SWS counts,<sup>32,67,105</sup> whereas inhibiting GABA<sub>B</sub>-receptor function dampens SWS.<sup>29,67,106</sup> The long-lasting and powerful inhibition produced by postsynaptic GABA<sub>B</sub> receptors recruits low threshold, T-type calcium channel activity to produce robust post-inhibitory rebound bursts that probably sustain SWS.<sup>5,65</sup> Consistent with these observations, we show that activated AMPK potentiates postsynaptic GABA<sub>B</sub>-receptor signalling in thalamocortical neurons; strengthens GABA<sub>B</sub>-receptor-dependent, epileptiform oscillations recorded in thalamic brain slice preparations and increases SWS. Postsynaptic GABA<sub>B</sub> receptors have a moderate affinity for GABA (1 μM<sup>107</sup>) and are largely localized to extrasynaptic dendritic regions of thalamocortical neurons.<sup>28</sup> Thus, the receptors are largely inactive during basal conditions or during moderate synaptic activity.<sup>108–110</sup> However, if GABAergic inputs are sufficiently active, then released GABA can spillover to extrasynaptic regions to activate GABA<sub>B</sub> receptors.<sup>75</sup> We propose that AMPK-mediated potentiation of thalamic GABA<sub>B</sub>-receptor activity during hypoglycaemia reduces the threshold for such receptor activation.

Herein, we focused on the potential contribution of the thalamus to hypoglycaemia-provoked SWS. Notably, however, SWS result from complex interactions between multiple structures, including the cortex and thalamus. According to the cortical focus theory, the somatosensory cortex provides the initiating drive to thalamic circuits that then generate hypersynchronous, rhythmic activity that is rapidly generalized throughout widespread regions of the cortex.<sup>111,112</sup> While our findings demonstrate that selective disruption of glucose metabolism in the thalamus is sufficient to elevate SWS in the seizure-prone animal, future studies are

warranted to determine whether selective cortical disruption is likewise sufficient. Nonetheless, our current observations suggest that glucose-sensitive mechanisms in the thalamus might establish a threshold necessary to produce generalized SWS, and that hypoglycaemia reduces this threshold by enhancing thalamic GABA<sub>B</sub>-receptor function. This hypothesis is consistent with the observation that the human thalamus is uniquely sensitive to even moderate levels of hypoglycaemia.<sup>113</sup>

### Metformin and spike-wave seizures

Metformin exacerbated SWS and, at high doses, evoked a profound and fatal seizure response in seizure-prone animals. Metformin inhibits complex I of the mitochondrial electron transport chain, an effect that reduces ATP production and elevates AMP levels that facilitate AMPK activation.<sup>82</sup> Metformin increases insulin sensitivity, enhances glucose uptake in muscle tissue, and blocks gluconeogenesis in the liver; collectively, all actions result in lower blood glucose<sup>82</sup> and make metformin the most common and highly effective pharmacological treatment for type 2 diabetes.<sup>82,114</sup> With its ability to pass the blood–brain barrier, metformin also has potential therapeutic effects in Huntington's disease,<sup>115</sup> Alzheimer's disease<sup>116</sup> and some forms of epilepsy.<sup>76–78,117</sup> While adverse actions of metformin on absence epilepsy are not reported, several reasons may obscure any possible links. First, the high metformin dose used in our study was roughly twice that of the equivalent dose used in humans and therefore may not have a clinical equivalence; however, metformin overdose occurs in humans.<sup>114,118</sup> Second, despite the drug's ubiquity, metformin is generally not prescribed to children; the mean age of onset for childhood absence epilepsy is 4–7 years of age.<sup>119</sup> Thus, future studies are required to fully resolve the clinical ramifications of our unexpected observations.

Herein, the effects of metformin on SWS probably result from a combination of actions. We propose that lower doses of metformin activate AMPK to augment GABA<sub>B</sub>-receptor mediated signalling and increase SWS. The actions of high doses of metformin are probably multifaceted. Following a high dose of metformin, SWS counts not only increased, but all animals quickly transitioned into a state of near-continuous spike-wave activity (i.e. absence status epilepticus). We speculate that metformin-induced absence status epilepticus in rats results from the converging and enhancing actions of AMPK<sup>27</sup> and lactate<sup>81</sup> on thalamic GABA<sub>B</sub>-receptor function. The subsequent progression into convulsive, tonic-clonic seizures (status epilepticus) and death probably results from the actions of elevated lactate on multiple brain structures. Indeed, the drug's capacity to produce lactic acidosis provides the basis for the FDA's black box warning. Nevertheless, the intense seizure response was not observed in non-epileptic Wistar rats. Thus, SWS predisposition appears necessary for a metformin-provoked seizure response. Clearly, the actions of metformin are complex and varied, and fully testing this hypothesis will ultimately benefit from transgenic approaches that modify AMPK's activation capability.

## Conclusions

In aggregate, our study addresses a growing number of observations that glucose availability regulates SWS. Despite such conclusions, the mechanisms that enable hypoglycaemia to regulate SWS remain entirely unknown. We now provide data in support of the hypothesis that glucose-mediated regulation of SWS results from p-AMPK potentiation of GABA<sub>B</sub>-receptor-mediated signalling.

## Acknowledgements

We are grateful to our UVa colleagues that assisted us with lively data discussions and technical expertise: Dr Ian E. Burbulis for guidance in molecular biology, John M. Williamson, for his guidance with acquiring rodent EEG, and Dr Ruth L. Stornetta and Dr Ronald P. Gaykema aided with immunohistochemical approaches. Last, Dr Michelle L. Bland, Dr Thurl E. Harris and Dr Eugene J. Barrett provided insight into AMPK and metformin biology. We also thank Dr Howard P. Goodkin for comments on early drafts of the manuscript.

## Funding

This study was funded by intramural support from the NIH funding agencies NINDS (R01 NS099586), NIAMS (R01 AR050429), NIDDK (K99/R00-AG057825), NIGMS (T32G007055) and the American Heart Association (#19POST34430205).

## Competing interests

The authors report no competing interests.

## Supplementary material

Supplementary material is available at *Brain* online.

## References

- Huguenard JR, McCormick DA. Thalamic synchrony and dynamic regulation of global forebrain oscillations. *Trends Neurosci.* 2007;30(7):350–356.
- McCafferty C, David F, Venzi M, et al. Cortical drive and thalamic feed-forward inhibition control thalamic output synchrony during absence seizures. *Nat Neurosci.* 2018;21(5):744–756.
- Kandel A, Buzsáki G. Cellular–synaptic generation of sleep spindles, spike-and-wave discharges, and evoked thalamocortical responses in the neocortex of the rat. *J Neurosci.* 1997;17(17):6783–6797.
- Avoli M. A brief history on the oscillating roles of thalamus and cortex in absence seizures. *Epilepsia.* 2012;53(5):779–789.
- Beenhakker MP, Huguenard JR. Neurons that fire together also conspire together: Is normal sleep circuitry hijacked to generate epilepsy? *Neuron.* 2009;62(5):612–632.
- Blumenfeld H. Cellular and network mechanisms of spike-wave seizures. *Epilepsia.* 2005;46:21–33.
- Meeren HKM, Pijn JPM, Van Luijckelaar ELJM, Coenen AML, da Silva FHL. Cortical focus drives widespread corticothalamic networks during spontaneous absence seizures in rats. *J Neurosci.* 2002;22(4):1480–1495.
- Mergenthaler P, Lindauer U, Dienel GA, Meisel A. Sugar for the brain: The role of glucose in physiological and pathological brain function. *Trends Neurosci.* 2013;36(10):587–597.
- Mullen SA, Berkovic SF. Genetic generalized epilepsies. *Epilepsia.* 2018;59(6):1148–1153.
- Leiva-Salinas C, Quigg M, Elias WJ, et al. Earlier seizure onset and longer epilepsy duration correlate with the degree of temporal hypometabolism in patients with mesial temporal lobe sclerosis. *Epilepsy Res.* 2017;138:105–109.
- Reid CA, Kim TH, Berkovic SF, Petrou S. Low blood glucose precipitates spike-and-wave activity in genetically predisposed animals. *Epilepsia.* 2011;52(1):115–120.
- Arsov T, Mullen SA, Rogers S, et al. Glucose transporter 1 deficiency in the idiopathic generalized epilepsies. *Ann Neurol.* 2012;72(5):807–815.
- Gibbs FA, Gibbs EL, Lennox WG. Influence of the blood sugar on the wave and spike formation in petit mal epilepsy. *Arch Neurol Psychiatry.* 1939;41(6):1111–1116.
- Leary LD, Wang D, Nordli DR, Engelstad K, De Vivo DC. Seizure characterization and electroencephalographic features in glut-1 deficiency syndrome. *Epilepsia.* 2003;44(5):701–707.
- Simpson IA, Appel NM, Hokari M, et al. Blood–brain barrier glucose transporter. *J Neurochem.* 1999;72(1):238–247.
- Simpson IA, Carruthers A, Vannucci SJ. Supply and demand in cerebral energy metabolism: The role of nutrient transporters. *J Cereb Blood Flow Metab.* 2007;27(11):1766–1791.
- Furuse T, Mizuma H, Hirose Y, et al. A new mouse model of GLUT1 deficiency syndrome exhibits abnormal sleep-wake patterns and alterations of glucose kinetics in the brain. *Dis Model Mech.* 2019;12(9):dmm038828.
- Dienel GA. Brain glucose metabolism: Integration of energetics with function. *Physiol Rev.* 2018;99(1):949–1045.
- López-Gamero AJ, Martínez F, Salazar K, Cifuentes M, Nualart F. Brain glucose-sensing mechanism and energy homeostasis. *Mol Neurobiol.* 2019;56:769–796.
- Yellen G. Ketone bodies, glycolysis, and K(ATP) channels in the mechanism of the ketogenic diet. *Epilepsia.* 2008;49(Suppl 8):80–82.
- Ashford ML, Boden PR, Treherne JM. Glucose-induced excitation of hypothalamic neurones is mediated by ATP-sensitive K<sup>+</sup> channels. *Pflugers Arch.* 1990;415(4):479–483.
- Tanner GR, Lutas A, Martínez-François JR, Yellen G. Single KATP channel opening in response to action potential firing in mouse dentate granule neurons. *J Neurosci.* 2011;31(23):8689–8696.
- Giménez-Cassina A, Martínez-François JR, Fisher JK, et al. BAD-dependent regulation of fuel metabolism and KATP channel activity confers resistance to epileptic seizures. *Neuron.* 2012;74(4):719–730.
- Lee K, Dixon AK, Richardson PJ, Pinnock RD. Glucose-receptive neurones in the rat ventromedial hypothalamus express KATP channels composed of Kir6.1 and SUR1 subunits. *J Physiol.* 1999;515(Pt 2):439–452.
- Karschin A, Brockhaus J, Ballanyi K. KATP channel formation by the sulphonylurea receptors SUR1 with Kir6.2 subunits in rat dorsal vagal neurons in situ. *J Physiol.* 1998;509(Pt 2):339–346.
- Martínez-François JR, Fernández-Agüera MC, Nathwani N, et al. BAD and KATP channels regulate neuron excitability and epileptiform activity. *eLife.* 2018;7:e32721.
- Kuramoto N, Wilkins ME, Fairfax BP, et al. Phospho-dependent functional modulation of GABAB receptors by the metabolic sensor AMP-dependent protein kinase. *Neuron.* 2007;53(2):233–247.
- Kulik Á, Nakadate K, Nyíri G, et al. Distinct localization of GABAB receptors relative to synaptic sites in the rat cerebellum and ventrobasal thalamus. *Eur J Neurosci.* 2002;15(2):291–307.
- Bortolato M, Frau R, Orrù M, et al. GABAB receptor activation exacerbates spontaneous spike-and-wave discharges in DBA/2J mice. *Seizure.* 2010;19(4):226–231.
- Destexhe A. Spike-and-wave oscillations based on the properties of GABAB receptors. *J Neurosci.* 1998;18(21):9099–9111.
- Hosford DA, Clark S, Cao Z, et al. The role of GABAB receptor activation in absence seizures of lethargic (lh/lh) mice. *Science.* 1992;257(5068):398–401.
- Vergnes M, Boehrer A, Simler S, Bernasconi R, Marescaux C. Opposite effects of GABAB receptor antagonists on absences and convulsive seizures. *Eur J Pharmacol.* 1997;332(3):245–255.

33. Krosigk MV, Bal T, McCormick DA. Cellular mechanisms of a synchronized oscillation in the thalamus. *Science*. 1993; 261(5119):361–364.
34. Blumenfeld H, McCormick DA. Corticothalamic inputs control the pattern of activity generated in thalamocortical networks. *J Neurosci*. 2000;20(13):5153–5162.
35. Bal T, Debay D, Destexhe A. Cortical feedback controls the frequency and synchrony of oscillations in the visual thalamus. *J Neurosci*. 2000;20(19):7478–7488.
36. Lu AC, Lee CK, Kleiman-Weiner M, et al. Nonlinearities between inhibition and T-type calcium channel activity bidirectionally regulate thalamic oscillations. *eLife*. 2020;9:e59548.
37. Laker RC, Drake JC, Wilson RJ, et al. AMPK phosphorylation of Ulk1 is required for targeting of mitochondria to lysosomes in exercise-induced mitophagy. *Nat Commun*. 2017;8(1):548.
38. Ting JT, Daigle TL, Chen Q, Feng G. Acute brain slice methods for adult and aging animals: application of targeted patch clamp analysis and optogenetics. In: Martina M, Taverna S, eds. *Patch-clamp methods and protocols. Methods in molecular biology*. Springer; 2014:221–242.
39. Sprenger JU, Perera RK, Götz KR, Nikolaev VO. FRET microscopy for real-time monitoring of signaling events in live cells using unimolecular biosensors. *J Vis Exp*. 2012;66:e4081.
40. Coenen AML, van Luijckelaar ELJM. Genetic animal models for absence epilepsy: a review of the WAG/Rij strain of rats. *Behav Genet*. 2003;33(6):635–655.
41. van Luijckelaar EL, Coenen AM. Two types of electrocortical paroxysms in an inbred strain of rats. *Neurosci Lett*. 1986;70(3):393–397.
42. Rehni AK, Dave KR. Impact of hypoglycemia on brain metabolism during diabetes. *Mol Neurobiol*. 2018;55(12):9075–9088.
43. Lutas A, Yellen G. The ketogenic diet: metabolic influences on brain excitability and epilepsy. *Trends Neurosci*. 2013;36(1):32–40.
44. Tokarz VL, MacDonald PE, Klip A. The cell biology of systemic insulin function. *J Cell Biol*. 2018;217(7):2273–2289.
45. Titchenell PM, Lazar MA, Birnbaum MJ. Unraveling the regulation of hepatic metabolism by insulin. *Trends Endocrinol Metab*. 2017;28(7):497–505.
46. Bieberdorf FA, Chernick SS, Scow RO. Effect of insulin and acute diabetes on plasma FFA and ketone bodies in the fasting rat. *J Clin Invest*. 1970;49(9):1685–1693.
47. Sherwin RS, Hendler RG, Felig P. Effect of diabetes mellitus and insulin on the turnover and metabolic response to ketones in man. *Diabetes*. 1976;25(9):776–784.
48. Vinué Á, González-Navarro H. Glucose and insulin tolerance tests in the mouse. In: Andrés V, Dorado B, eds. *Methods in mouse atherosclerosis. Methods in molecular biology*. Springer; 2015:247–254.
49. Routh VH, Hao L, Santiago AM, Sheng Z, Zhou C. Hypothalamic glucose sensing: making ends meet. *Front Syst Neurosci*. 2014;8:236.
50. Arbeláez AM, Rutlin JR, Hershey T, Powers WJ, Videen TO, Cryer PE. Thalamic activation during slightly subphysiological glycemia in humans. *Diabetes Care*. 2012;35:2570–2574.
51. Wick AN, Drury DR, Nakada HI, Wolfe JB. Localization of the primary metabolic block produced by 2-deoxyglucose. *J Biol Chem*. 1957;224(2):963–969.
52. Fogerson PM, Huguenard JR. Tapping the brakes: Cellular and synaptic mechanisms that regulate thalamic oscillations. *Neuron*. 2016;92(4):687–704.
53. Slusser PG, Ritter RC. Increased feeding and hyperglycemia elicited by intracerebroventricular 5-thiogluconic acid. *Brain Res*. 1980; 202(2):474–478.
54. Kahn BB, Alquier T, Carling D, Hardie DG. AMP-activated protein kinase: Ancient energy gauge provides clues to modern understanding of metabolism. *Cell Metab*. 2005;1(1):15–25.
55. Herzig S, Shaw RJ. AMPK: Guardian of metabolism and mitochondrial homeostasis. *Nat Rev Mol Cell Biol*. 2018;19(2):121–135.
56. Culmsee C, Monnig J, Kemp BE, Mattson MP. AMP-activated protein kinase is highly expressed in neurons in the developing rat brain and promotes neuronal survival following glucose deprivation. *J Mol Neurosci*. 2001;17(1):45–58.
57. Kim EK, Miller I, Aja S, et al. C75, a fatty acid synthase inhibitor, reduces food intake via hypothalamic AMP-activated protein kinase. *J Biol Chem*. 2004;279(19):19970–19976.
58. Lee K, Li B, Xi X, Suh Y, Martin RJ. Role of neuronal energy status in the regulation of adenosine 5'-monophosphate-activated protein kinase, orexigenic neuropeptides expression, and feeding behavior. *Endocrinology*. 2005;146(1):3–10.
59. McCrimmon RJ, Fan X, Ding Y, Zhu W, Jacob RJ, Sherwin RS. Potential role for AMP-activated protein kinase in hypoglycemia sensing in the ventromedial hypothalamus. *Diabetes*. 2004;53(8):1953–1958.
60. Ramamurthy S, Ronnett GV. Developing a head for energy sensing: AMP-activated protein kinase as a multifunctional metabolic sensor in the brain. *J Physiol*. 2006;574(1):85–93.
61. Li J, Zeng Z, Viollet B, Ronnett GV, McCullough LD. Neuroprotective effects of adenosine monophosphate-activated protein kinase inhibition and gene deletion in stroke. *Stroke*. 2007;38(11):2992–2999.
62. Kong D, Dagon Y, Campbell JN, et al. A postsynaptic AMPK→p21-activated kinase pathway drives fasting-induced synaptic plasticity in AgRP neurons. *Neuron*. 2016;91(1):25–33.
63. Tsou P, Zheng B, Hsu CH, Sasaki AT, Cantley LC. A fluorescent reporter of AMPK activity and cellular energy stress. *Cell Metab*. 2011;13(4):476–486.
64. Konagaya Y, Terai K, Hirao Y, et al. A highly sensitive FRET biosensor for AMPK exhibits heterogeneous AMPK responses among cells and organs. *Cell Rep*. 2017;21(9):2628–2638.
65. McCormick DA, Contreras D. On the cellular and network bases of epileptic seizures. *Annu Rev Physiol*. 2001;63(1):815–846.
66. Padgett CL, Slesinger PA. GABAB receptor coupling to G-proteins and ion channels. In: Thomas PB, ed. *Advances in pharmacology*, Vol. 58. Academic Press; 2010:123–147.
67. Liu Z, Vergnes M, Depaulis A, Marescaux C. Involvement of intrathalamic GABAB neurotransmission in the control of absence seizures in the rat. *Neuroscience*. 1992;48(1):87–93.
68. Couve A, Thomas P, Calver AR, et al. Cyclic AMP-dependent protein kinase phosphorylation facilitates GABAB receptor-effector coupling. *Nat Neurosci*. 2002;5(5):415–424.
69. Zhou G, Myers R, Li Y, et al. Role of AMP-activated protein kinase in mechanism of metformin action. *J Clin Invest*. 2001; 108(8):1167–1174.
70. Göransson O, McBride A, Hawley SA, et al. Mechanism of action of A-769662, a valuable tool for activation of AMP-activated protein kinase. *J Biol Chem*. 2007;282(45):32549–32560.
71. von Krosigk M, Bal T, McCormick DA. Cellular mechanisms of a synchronized oscillation in the thalamus. *Science*. 1993;261(5119):361–364.
72. Bal T, von Krosigk M, McCormick DA. Synaptic and membrane mechanisms underlying synchronized oscillations in the ferret lateral geniculate nucleus in vitro. *J Physiol*. 1995;483(3):641–663.
73. Kleiman-Weiner M, Beenhakker MP, Segal WA, Huguenard JR. Synergistic roles of GABAA receptors and SK channels in regulating thalamocortical oscillations. *J Neurophysiol*. 2009;102(1): 203–213.
74. Bryant AS, Li B, Beenhakker MP, Huguenard JR. Maintenance of thalamic epileptiform activity depends on the astrocytic glutamate-glutamine cycle. *J Neurophysiol*. 2009;102(5):2880–2888.
75. Beenhakker MP, Huguenard JR. Astrocytes as gatekeepers of GABAB receptor function. *J Neurosci*. 2010;30(45):15262–15276.
76. Mehrabi S, Sanadgol N, Barati M, et al. Evaluation of metformin effects in the chronic phase of spontaneous seizures in

- pilocarpine model of temporal lobe epilepsy. *Metab Brain Dis*. 2018;33(1):107–114.
77. Osornio MDCR, Custodio Ramírez V, Calderón Gámez D, et al. Metformin plus caloric restriction show anti-epileptic effects mediated by mTOR pathway inhibition. *Cell Mol Neurobiol*. 2018;38(7):1425–1438.
  78. Zhao RR, Xu XC, Xu F, et al. Metformin protects against seizures, learning and memory impairments and oxidative damage induced by pentylenetetrazole-induced kindling in mice. *Biochem Biophys Res Commun*. 2014;448(4):414–417.
  79. Festing MFW. Inbred strains of rats. In: Festing MFW, ed. *Inbred strains in biomedical research*. Macmillan Education; 1979:267–296.
  80. Huang W, Castelino RL, Peterson GM. Lactate levels with chronic metformin use: A narrative review. *Clin Drug Investig*. 2017;37(11):991–1007.
  81. Abrantes HDC, Briquet M, Schmuziger C, et al. The lactate receptor HCAR1 modulates neuronal network activity through the activation of Gα and Gβγ subunits. *J Neurosci*. 2019;39(23):4422–4433.
  82. Pernicova I, Korbonits M. Metformin—mode of action and clinical implications for diabetes and cancer. *Nat Rev Endocrinol*. 2014;10(3):143–156.
  83. Schousboe A, Bak LK, Sickmann HM, Sonnewald U, Waagepetersen HS. Energy substrates to support glutamatergic and GABAergic synaptic function: Role of glycogen, glucose and lactate. *Neurotox Res*. 2007;12(4):263–268.
  84. Wang D, Pascual JM, De Vivo D. Glucose transporter type 1 deficiency syndrome. In: Adam MP, Ardinger HH, Pagon RA, et al., eds. *GeneReviews®*. University of Washington; 1993.
  85. Soto-Insuga V, López RG, Losada-Del Pozo R, et al. Glut1 deficiency is a rare but treatable cause of childhood absence epilepsy with atypical features. *Epilepsy Res*. 2019;154:39–41.
  86. Kristopher JB, Carl ES. The ketogenic diet. In: *Epilepsy*. CRC Press; 2010:417–439.
  87. Meira IDA, Romão TT, Pires do Prado HJ, Krüger LT, Pires MEP, da Conceição PO. Ketogenic diet and epilepsy: What we know so far. *Front Neurosci*. 2019;13:5.
  88. Liu H, Yang Y, Wang Y, et al. Ketogenic diet for treatment of intractable epilepsy in adults: A meta-analysis of observational studies. *Epilepsia Open*. 2018;3(1):9–17.
  89. McNally MA, Hartman AL. Ketone bodies in epilepsy. *J Neurochem*. 2012;121(1):28–35.
  90. Kadowaki A, Sada N, Juge N, Wakasa A, Moriyama Y, Inoue T. Neuronal inhibition and seizure suppression by acetoacetate and its analog, 2-phenylbutyrate. *Epilepsia*. 2017;58(5):845–857.
  91. Ma W, Berg J, Yellen G. Ketogenic diet metabolites reduce firing in central neurons by opening KATP channels. *J Neurosci*. 2007; 27(14):3618–3625.
  92. Grooms LB, Pyzik PL, Turner Z, Dorward JL, Goode VH, Kossoff EH. Do patients with absence epilepsy respond to ketogenic diets? *J Child Neurol*. 2011;26(2):160–165.
  93. Thampongkol S, Vears DF, Bicknell-Royle J, et al. Efficacy of the ketogenic diet: Which epilepsies respond? *Epilepsia*. 2012;53(3): e55–e59.
  94. Garriga-Canut M, Schoenike B, Qazi R, et al. 2-Deoxy-D-glucose reduces epilepsy progression by NRSF-CtBP-dependent metabolic regulation of chromatin structure. *Nat Neurosci*. 2006;9(11):1382–1387.
  95. Rho JM, Shao LR, Stafstrom CE. 2-Deoxyglucose and beta-hydroxybutyrate: Metabolic agents for seizure control. *Front Cell Neurosci*. 2019;13:172.
  96. Liu L, Zheng T, Morris MJ, et al. The mechanism of carbamazepine aggravation of absence seizures. *J Pharmacol Exp Ther*. 2006;319(2):790–798.
  97. Panayiotopoulos CP. Typical absence seizures and their treatment. *Arch Dis Child*. 1999;81(4):351–355.
  98. Panayiotopoulos CP, Agathonikou A, Sharoqi IA, Parker AP. Vigabatrin aggravates absences and absence status. *Neurology*. 1997;49(5):1467.
  99. Parker AP, Agathonikou A, Robinson RO, Panayiotopoulos CP. Inappropriate use of carbamazepine and vigabatrin in typical absence seizures. *Dev Med Child Neurol*. 1998;40(8):517–519.
  100. Schapel G, Chadwick D. Tiagabine and non-convulsive status epilepticus. *Seizure*. 1996;5(2):153–156.
  101. Gelisse P, Genton P, Kuate C, Pesenti A, Baldy-Moulinier M, Crespel A. Worsening of seizures by oxcarbazepine in juvenile idiopathic generalized epilepsies. *Epilepsia*. 2004;45(10):1282–1286.
  102. French JA, Pedley TA. Clinical practice. Initial management of epilepsy. *N Engl J Med*. 2008;359:166–176.
  103. Osorio I, Reed RC, Peltzer JN. Refractory idiopathic absence status epilepticus: A probable paradoxical effect of phenytoin and carbamazepine. *Epilepsia*. 2000;41(7):887–894.
  104. Knake S, Hamer HM, Schomburg U, Oertel WH, Rosenow F. Tiagabine-induced absence status in idiopathic generalized epilepsy. *Seizure*. 1999;8(5):314–317.
  105. Smith KA, Fisher RS. The selective GABAB antagonist CGP-35348 blocks spike-wave bursts in the cholesterol synthesis rat absence epilepsy model. *Brain Res*. 1996;729(2):147–150.
  106. Stewart LS, Wu Y, Eubanks JH, et al. Severity of atypical absence phenotype in GABAB transgenic mice is subunit specific. *Epilepsy Behav*. 2009;14(4):577–581.
  107. Sodickson DL, Bean BP. GABAB receptor-activated inwardly rectifying potassium current in dissociated hippocampal CA3 neurons. *J Neurosci*. 1996;16(20):6374–6385.
  108. Dutar P, Nicoll RA. Pre- and postsynaptic GABAB receptors in the hippocampus have different pharmacological properties. *Neuron*. 1988;1(7):585–591.
  109. Scanziani M. GABA spillover activates postsynaptic GABAB receptors to control rhythmic hippocampal activity. *Neuron*. 2000;25(3):673–681.
  110. Kim U, Sanchez-Vives MV, McCormick DA. Functional dynamics of GABAergic inhibition in the thalamus. *Science*. 1997;278(5335):130–134.
  111. Manning JPA, Richards DA, Leresche N, Crunelli V, Bowery NG. Cortical-area specific block of genetically determined absence seizures by ethosuximide. *Neuroscience*. 2004;123(1):5–9.
  112. Meeren HKM, Pijn JPM, Van Luijckelaar ELJM, Coenen AML, da Silva FHL. Cortical focus drives widespread corticothalamic networks during spontaneous absence seizures in rats. *J Neurosci*. 2002;22(4):1480–1495.
  113. Arbeláez AM, Rutlin JR, Hershey T, Powers WJ, Videen TO, Cryer PE. Thalamic activation during slightly subphysiological glycemia in humans. *Diabetes Care*. 2012;13:2570–2574.
  114. Flory J, Lipska K. Metformin in 2019. *JAMA*. 2019;321(19):1926–1927.
  115. Ma TC, Buescher JL, Oatis B, et al. Metformin therapy in a transgenic mouse model of Huntington's disease. *Neurosci Lett*. 2007; 411(2):98–103.
  116. Li J, Deng J, Sheng W, Zuo Z. Metformin attenuates Alzheimer's disease-like neuropathology in obese, leptin-resistant mice. *Pharmacol Biochem Behav*. 2012;101(4):564–574.
  117. Yang Y, Zhu B, Zheng F, et al. Chronic metformin treatment facilitates seizure termination. *Biochem Biophys Res Commun* 2017; 484(2):450–455.
  118. Chiew AL, Wright DFB, Dobos NM, et al. "Massive" metformin overdose. *Br J Clin Pharmacol*. 2018;84(12): 2923–2927.
  119. Matricardi S, Verrotti A, Chiarelli F, Cerminara C, Curatolo P. Current advances in childhood absence epilepsy. *Pediatr Neurol*. 2014;50(3):205–212.